MSc thesis in Geomatics

CFD, sensitivity analysis, and optimisation to promote the formation of dunes

Nadine Hobeika
2021

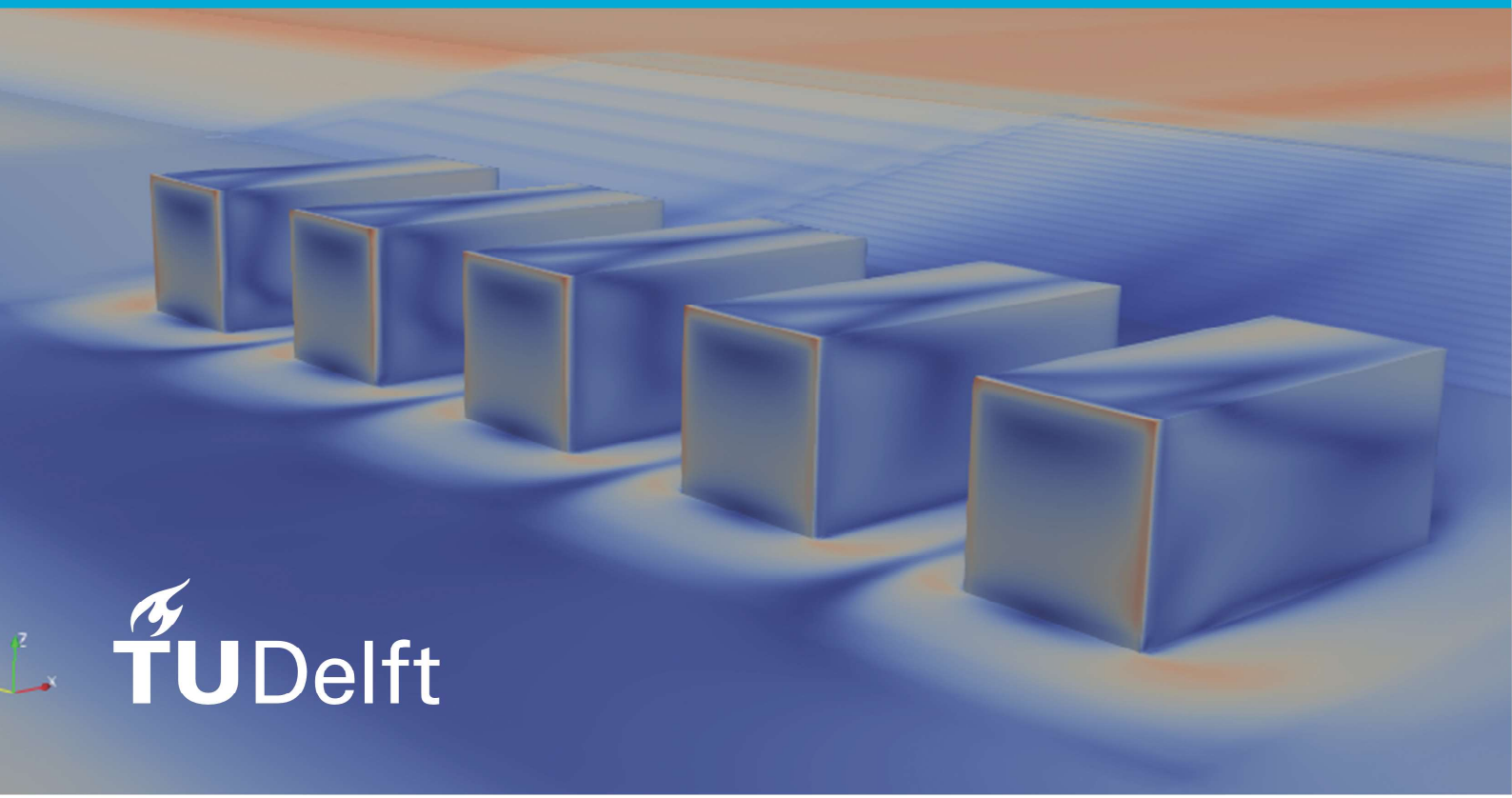

TU Delft

MSc thesis in Geomatics

CFD, sensitivity analysis and optimisation to promote the formation of dunes

Nadine Hobeika

July 2021

A thesis submitted to the Delft University of Technology in partial fulfillment of the requirements for the degree of Master of Science in Geomatics

The work in this thesis was carried out in the:

3D geoinformation group
Delft University of Technology

Supervisors: Dr. Clara García-Sánchez
Ivan Pađen
Co-reader: Stelios Vitalis

Abstract

In 2017, the 'Kustpact', a Dutch national agreement, was signed to develop the Dutch coast without damaging its ecosystem nor its aesthetics. Consequently, the formation and protection of coastal dunes have become a focal point for research and development. For this reason, based on the idea of Performance-Based Design (PBD), this Master thesis aims to investigate the impact of certain geometric design parameters of beach house configurations on wind turbulence for the purpose of widening the dunes.

A parametric design space was set up to easily automate Computational Fluid Dynamics (CFD) simulations for different purposes throughout this study. The sediment mobility estimation was the objective function for all simulations conducted. It is based on the difference of transport rate between two lines from the beginning of the plateau to the foot of the dunes. To simplify the parametric model, a Sensitivity Analysis (SA) was conducted to statistically identify the most influential parameters in the model. Afterward, the filtered parameters from the SA are used to build a surrogate model to detect the trends that result from combining the most influential parameters. Finally, a Surrogate-Based Optimisation (SBO) is conducted based on the former surrogate and using a Genetic Algorithm (GA). Three generations were run and used to increase the accuracy of the surrogate and predict an optimum solution for widening the dunes.

The study concludes on a list of design criteria to respect in order to widen the dunes mainly pertaining to the consistent position of the configuration relative to the dunes, the important overlap between houses and the larger wind-facing direction of the configuration.

Acknowledgements

First, I would like to thank my supervisors, Dr. Clara García-Sánchez and Ivan Pađen, for your support throughout this year. Our discussions helped untangle the mess that would grow in my head throughout the week. No matter how big the issue was, you always made me feel that I can easily overcome it. Thank you for meeting my enthusiasm with your enthusiasm and your trust in my capabilities. I also want to thank Stelios Vitalis for his valuable insights on my report.

Second, I would like to thank the 3D geoinformation group for giving me access to their clusters (Godzilla and Gilfoyle). Without those clusters, none of this work would have been possible. I would also like to thank the Shorescape team for allowing me to work on the project.

Finally, I would like to thank my parents, my siblings, my aunts, and my dearest friend for always being there and pretending to understand what I was talking about this whole year. I appreciate how much you believe in me, and I hope I keep making you proud. I would also like to thank all my friends around the world. The pandemic might have separated us physically, but our video calls were the perfect vent-off in this crazy year.

Contents

List of Figures

List of Tables

List of Algorithms

Acronyms

1 Introduction

Ever since the first industrial revolution at the end of the 18th century, the impact of human activities on climate change has become more apparent and the issue keeps growing at a fast pace. For example, satellite observations show that the multi-year Arctic ice is currently shrinking by 13.1% per decade, compared to the average between 1981 and 2010 [Change, 2021]. Even if the temperature no longer increases, the meltdown of glaciers is inevitable [Huybrechts, 2013]. The most immediate result of large-scale melting ice is the rise of sea level, increasing coastal hazards and consequently threatening the expansion of human activities. However, at the same time, the urban population, which is projected to cover 68% of the global population in 2050, tends to concentrate in coastal areas. This increases vulnerability and exposure of urban communities. Figure 1.1 shows the vicious cycle from more intensive human activities. A more resilient approach needs to be established to better cope with the imminent danger.

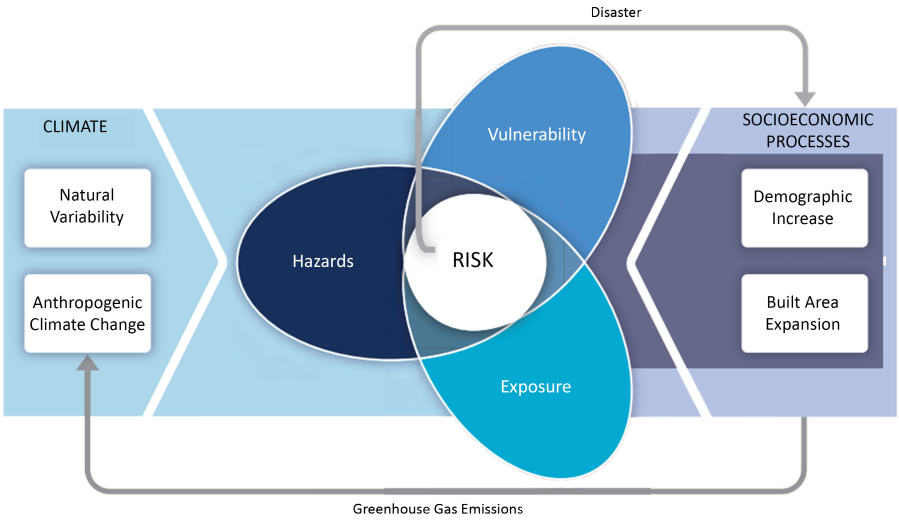

Figure 1.1: Current risk cycle between socioeconomic processes and climate change. Source: adapted from [Lavell et al., 2012]

In the Netherlands, this dilemma is particularly relevant with the territory mostly lying under sea level and the ever-growing population expanding towards at-risk areas. Another Dutch coast particularity is their natural defence system based on the formation of dunes. These defences are threatened both by climate change and demographic expansion. Consequently, in 2017, the 'Kuspact', a Dutch national agreement, was signed to develop the Dutch coast without damaging its ecosystem nor its aesthetics and maintaining the coastal line of defence against floods in the most natural way possible [Schultz van Haegen, M.H., 2017].

One result of the agreement is the Shorescape project, joint research between the department of Urbanism at the Delft University of Technology and the Department of Water Engineering and Management at the University of Twente. The agreement is in line with the Building with Nature (BwN) concept where natural dynamics are studied to mitigate the impact of human activities in the environment and to be able to integrate natural ecosystems without causing them harm. Among the natural dynamics, this

thesis will focus on the interaction between wind, dunes, and beach houses to promote the formation of dunes. The formation of dunes can be attained either by widening and/or heightening the dunes. In fact, this explores a PBD of beach house configurations.

PBD is a goal-oriented design that converges towards a performance-related criterion [Oxman, 2008]. In this case, the criterion will only address sediment mobility for widening the dunes; however, for heightening the dunes, nothing other than maximising or minimising the convergence criterion changes in the process. With the development of computational power, automatically running numerical simulations for PBD is essential to cover all the possible solutions efficiently. This means that a relevant number of simulations needs to be conducted to assess the criterion. For the purpose of this study, first, a parametric geometry is created to generate the needed configurations. Then, the geometry undergoes two processes both running a CFD process to generate the output. The first process is a SA that filters the least influential parameters. The second is a SBO that searches and concludes for the best configuration based on the performance criterion chosen.

1.1 Research questions

This thesis will focus on the main research question: *Based on wind simulation, which beach house configuration best promotes widening of dunes?*

Consequently, several sub-questions will also be explored to better answer the main research question. In dissecting the first question, three aspects can be extracted to create three categories of sub-questions. The three aspects are as follows: the wind simulation, the housing configurations, and the formation of dunes.

Wind simulation

- What is a suitable computational domain and mesh for the scenarios to be tested?

Housing configurations

- What are the parameters to define these house configurations?
- Which parameters are more influential on the formation of the dunes?

Formation of dunes

- How to factor in the wind direction in the final configuration choice?
- How to evaluate the widening of the dunes?

1.2 Thesis outline

This study is organised as follows:

- Chapter 2 consists of the theoretical background and related work that provides an overview of commonly used approaches in wind studies. It introduces the two main approaches, experimental and numerical, then, goes over the different methods in each approach. This chapter presents the advantages and disadvantages of each method and model to later motivate the decisions made during this research. It also discusses the theory behind sediment mobility. Afterward, it explains what are the processes and analysis methods that will be used during the study. It introduces both the SA and the optimisation and gives an overview of different approaches for each process.

- Chapter 3 presents the methodology followed in this work and then thoroughly goes over all the set-up decisions and details that will lead to a valid outcome. It defines the study area. It also introduces the geometric parameters and the wind properties used as input in this work and how and why they are chosen. It also explains the CFD implementation from governing equations to setting up the computational domain to validating the results. Finally, it explains the choice of SA and optimisation methods adopted.
- Chapter 4 goes over the results and discusses the output in the context of the research question. It concludes with the answer to the main research question. It also gives the trend with different combination of input variables.
- Chapter 5 concludes on the overall work process and the results, assesses the limitations of this study and whether the research questions have been answered, and finally proposes possible future work.

2 Theoretical background and related work

2.1 Overview of wind study approaches

In the atmospheric boundary layer, winds are turbulent with large and small vortices that change intensity and direction over time. Exactly modelling these vortices is still challenging; therefore, these vortices are estimated. There are different approaches to model the vortices and conduct wind studies in built environments (see Figure 2.1). The choice of approach depends on the available input and the desired output. This section gives an overview of the different approaches along with their advantages and disadvantages.

2.1.1 Experimental approach

The experimental approach consists of measurements in the physical world that are performed over time. The result is a mean flow field averaged over time. There are two types of experimental approaches for wind studies: field measurements and wind tunnel tests.

2.1.1.1 Field measurements

Field measurements provide the most realistic data about wind speed and direction under natural conditions, given that the used instruments give accurate measures. Measured data is the result of varying incident wind conditions, topographic changes, and different surface roughness lengths [Smyth, 2016]. The advantages of field measurements are that data is collected under real conditions and that measures in the real world do not suffer from any model scaling problems that occur in other wind study approaches.

However, field measurements rely on a limited number of anemometers which hinders the possibility of getting an entire flow field. More anemometers also increase the cost of field measurements, making it sometimes an expensive choice for a study [Wang, 2015]. Moreover, the impact of future projects and changes need to be predicted and hence cannot be measured on-site. Finally, wind conditions cannot be controlled thus making it difficult to study a specific condition or scenario [Wang, 2015]. Usually, field measures are used to validate wind tunnel tests or numeric simulations [Blocken, 2015].

2.1.1.2 Wind tunnel tests

Wind tunnel tests for the built environment are the reproduction of the Atmospheric Boundary Layer (ABL) characteristic profile on a scaled-down model to assess the impact of wind in a certain context. In order to achieve the desired ABL with the respective wind speed and turbulence intensities, specific features are mounted in front of the studied model, such as spires, barriers, carpets, and distributed roughness elements [Talamelli et al., 2004].

One important advantage of wind tunnel tests is the ability to control boundary conditions in the tunnel. It is also suitable to test different wind directions with the help of a turntable mounted in the tunnel and test different configurations through different models. Nevertheless, some issues arise when scaling down the model especially for small openings and small details. Since scaled-down models are a

simplification and an abstraction of the geometric reality of the built environment, it is challenging to achieve identical geometrical properties. It is also not always possible to reach the dynamic similarity requirements between the real-life situation and the wind-tunnel model such as the Reynolds number [Wang, 2015]. Wind tunnel tests are also used as a validation tool for numeric simulations [Hesp and Smyth, 2019].

2.1.2 Numeric approach

The numeric approach solves mathematical equations and sometimes models part of the wind properties in order to study the impact of wind in a certain context. There are different numeric approaches to study wind flow; the approaches presented below are the most common to use to study the impact of wind on aeolian landforms and/or buildings.

2.1.2.1 CFD simulations

CFD solves systems of nonlinear partial differential equations. There is no analytical solution in the general case and the final output goes through iterative numerical approaches [Cavaglieri, 2016]. There are many advantages for CFD simulations. The simulations are conducted at full scale, avoiding all scaling problems that might occur in wind tunnel tests. These simulations also provide full control over boundary conditions and output whole-flow field data. Moreover, CFD simulations allow the study of future projects and the easy testing of different parameters that affect these projects [Wang, 2015]. However, no mathematical equation can guarantee the stability, accuracy, and convergence of the results; therefore, validation and verification are essential before using the results of simulations [Blocken, 2015].

There are two types of approaches for CFD simulation: Direct Numerical Simulation (DNS) and simulation with turbulence modelling. Within the modelling simulations, there are the Large Eddy Simulation (LES) model and the Reynolds-Averaged Navier-Stokes (RANS) models.

DNS solves all the Navier-Stokes equations without a turbulence model. The calculation must solve all the spatial and temporal scales of the flow, accounting for all eddies; thus, the spatial and temporal resolution must be very high [Wang, 2015]. Therefore, DNS requires a great amount of computing power and remains favoured for cases with a low Reynolds number. For wind flow around buildings, Reynolds numbers are often very high making DNS prohibitively expensive [Smyth, 2016].

LES uses a spatial filter where large eddies are solved, and small eddies are modelled. This method is mostly used to solve unsteady flow. Generally, this model is very suitable for wake flow and remains advantageous for transient flow, around or behind an obstacle, which cannot be simulated by steady RANS models [Chaouat, 2017].
This approach requires meshes significantly finer than those used for RANS calculations. In addition, because it is designed to resolve unsteady flow, it should be run for a sufficiently long time to obtain converged results of the modelled flow [Blocken, 2018]. The power and computation time required are lower than for the DNS approach. However, because of the high computation time, the use of LES in studies around buildings or over aeolian landforms is still rare. Several papers do indicate that, with the evolution of computation capacity, the use of LES will become more common [Georgiadis et al., 2010; Piomelli, 2014; Blocken, 2015]. There are different LES models such as the Dutch Atmospheric Large Eddy Simulation (DALES). DALES extends the standard LES model to be suitable for flow over "sloping or heterogeneous terrain" like the dunes' morphology [Heus et al., 2010].

RANS Based on the Navier-Stokes equations, Osborne Reynolds proposed a decomposition where the instantaneous fluid speed is decomposed into a mean component and a fluctuating component. These equations can be used with approximations based on knowledge of the properties of flow turbulence, to give time-averaged solutions of turbulent flows [Wang, 2015].

Various turbulence models approximate the fluctuating component in the equations, such as k-ϵ turbulence models and k-ω turbulence models. Blocken et al. [2011] found that steady RANS models can produce accurate results (10-20%) in areas of high-speed wind. Even though the various RANS models develop and offer improvements, the main limitation of these models remains their inability to model the transient characteristics of the flow field such as separation and recirculation downstream of the edges and the formation of eddies in the wake [Blocken et al., 2011].

There is no general rule for choosing the best turbulence model. However, based on multiple papers that compare different models in different settings, an optimal choice can be made based on what suits the studied scenario best [Wang, 2015; Smyth, 2016; Hesp and Smyth, 2019].

1. RANS - Standard k-ϵ model: As a semi-empirical model, the Standard k-ϵ model is very popular due to its robustness, low run-time, and reasonable accuracy for a wide range of turbulent flows and heat transfer simulations. It integrates two partial differential transport equations in addition to the Navier Stokes equations for the description of turbulence, respectively, one on kinetic energy (k) and the other on the rate of dissipation of turbulence (ϵ) [Valen-Sendstad et al., 2013]. However, for flow around buildings, the standard model poses several problems. It is possible to have an overestimation of turbulent kinetic energy near the frontal area of the building resulting in an underestimation of the size of the separation and the regions of recirculation on the top and side faces of the building and an underestimation of the turbulent kinetic energy in the wake leading to an overestimation of the size of turbulence in the wake area. Consequently, based on the standard model, other models are developed, such as the ReNormalised Group (RNG) k-ϵ model and the k-ω turbulence models [Wang, 2015].

2. RANS - RNG k-ϵ model: This model is calculated using a statistical technique called the renormalisation group theory. Compared with the standard model, the RNG model improves the accuracy in the cases of:

   - High aerodynamic curvature and high deformation rate;
   - Transient flow and flow separation;
   - Heat and mass transfer and close to the wall;
   - Time-dependent flow with large scale movements [Thet and San, 2017]

   According to several papers, these improvements in the RNG model makes it the most suited RANS model for wind studies around buildings [Smyth, 2016; van Onselen, 2018; Hesp and Smyth, 2019].

3. RANS - k-ω turbulence models: k-ω turbulence models adopt a modified turbulent kinetic energy equation from the standard k-ϵ model and introduce a new equation for ω. The k-ω model incorporates modifications for low Reynolds number effects. The rates of propagation of free shear flows are in close agreement with measurements for distant wakes, mixed layers, and flat, round and radial jets. Therefore, it is applicable to flow limited by walls and free shear flows [Wang, 2015].

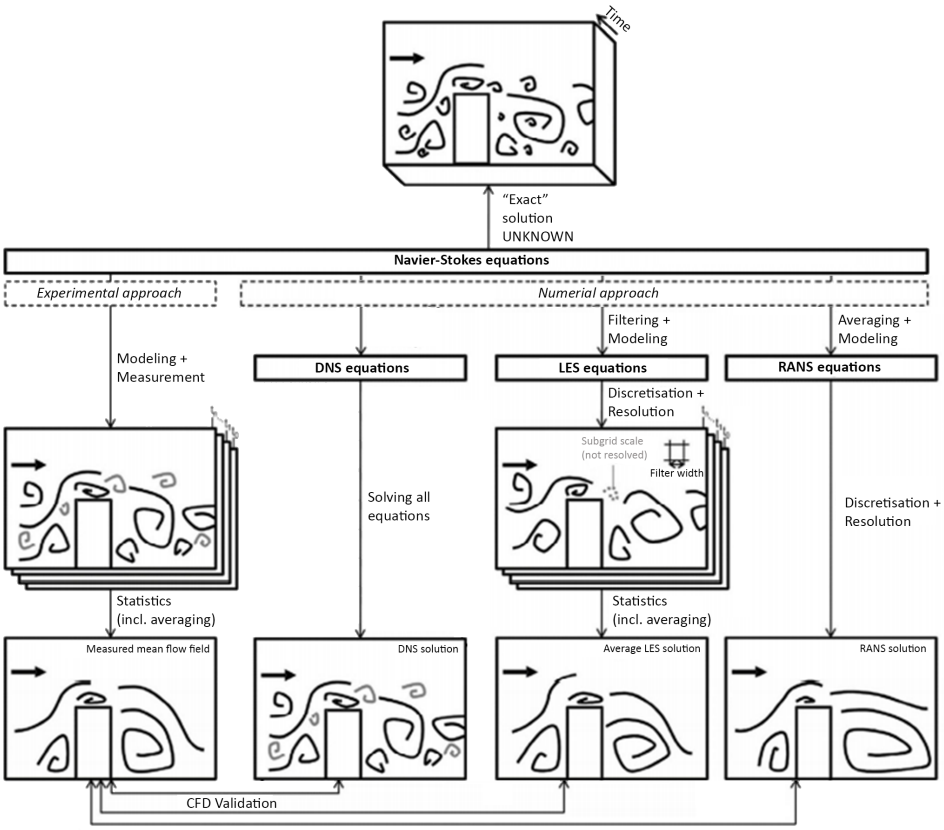

Figure 2.1: Overview of wind analysis approaches. Source: adapted from P. Gousseau's diagram in [Blocken, 2018]

2.1.2.2 Lattice Gas Cellular Automata (LGCA)

Mainly, used for wind studies around aeolian landforms, LGCA is based on a structured grid of cells each in a state (empty or full) and whose state may change over time. Unlike the kinetic theory of gases where space and time are continuous and where only the space of velocities is discrete, LGCA is completely discrete. The model is based on a few simple rules: identical particles, all of the same mass; collision rules for two or three particles respecting the conservation of the number of particles and their momentum; and an exclusion principle, that is, two particles on the same site at the same time cannot go in the same direction [Judice et al., 2007]. These principles are enough to find the main dynamic characteristics of a flow. LGCA is more efficient than CFD mainly because it uses integer arithmetic instead of floating-point operations. However, in 3D, these models become prohibitively expensive [Smyth, 2016].

2.2 Sediment mobility

Coastal dune systems are sandy sedimentary accumulations, typically of aeolian origin, dependent on sediment source areas, such as sandy beaches. This system relies on sediment mobility that is divided, based on the particle's size, into three categories by Bagnold [1941]:

- Creep ($>$ 500 µm);
- Saltation (70 - 500 µm);
- Suspension ($<$ 70 µm). [Nickling and Neuman, 2009]

Saltation alone is estimated to be responsible for 95% of sediment mobility making it the focus of aeolian landform studies [Nickling and Neuman, 2009]. Several field experiments indicate that sediment mobility by saltation can best be measured at a height lower than 50 cm [Arens et al., 2002; Mikami et al., 2005]

2.2.1 Factors for sediment mobility

Three fundamental factors condition sediment mobility: wind, beach morphology, and vegetation.

Wind For the wind factor, two important aspects affect sediment mobility: direction, and speed.

- Wind direction: is an important factor in sediment transport. In fact, land winds are normally less intense than sea winds and thus usually only change the shape of dunes and not their formation. Moreover, oblique sea winds carry the greatest quantities of sediment and cause significant morphodynamic variations [Nordstrom et al., 1996].
- Wind speed: there is a critical threshold from which the wind can transport sediments. The threshold is a function of the size of the particles, their density, and their cohesion [Bagnold, 1941]. For sandy shores, the minimum speed is $8\,\mathrm{m\,s^{-1}}$, a speed corresponding to degree 5 on the Beaufort scale.

Beach morphology The beach represents the sediment source for coastal wind transport. Wind movements of sand are potentially greater on wide, gently-sloped beaches than on narrow, steep-sloped beaches [Amrouni, 2002].

Vegetation Vegetation constitutes an important condition for the creation of dunes by trapping the particles of sand. The presence of vegetation is known to be one of the main factors limiting erosion. For winds up to $15\,\mathrm{m\,s^{-1}}$, it is estimated that the wind transport becomes zero when the vegetation cover reaches 43% [Amrouni, 2002].

2.3 Design and Analysis of Computer Experiments (DACE)

Numeric approaches to modelling physical processes mainly aim to automatically test different input variables and analyse how the output changes without the hassle of creating a large number of real-life models. However, the real world comes with a certain degree of randomness and uncertainty that needs to be accounted for in numeric approaches. This has lead scientists to create the Design and Analysis of Computer Experiments (DACE) which aims to detect trends in a parametric design space with a minimum number of samples [Adams et al., 2014]. DACE is usually used for different processes such as SA, uncertainty quantification and building surrogate models. This study will, first, use a SA to determine the most influential parameters and filter them before running the optimisation. Second, it will build an inexpensive surrogate model to be used for the optimisation.

Setting up a DACE consists of three main steps:

1. identifying relevant input parameters
2. sampling combinations of those parameters;
3. evaluating or using samples, depending on the chosen process.

2.3.1 Identifying relevant input parameters

The first step is to identify the input parameters, whether they are static or dynamic, and to model them by random variables. There are different ways to identify those parameters: experimental observations, previous studies, theoretical arguments, regulations, etc. Once input parameters are identified, their extent should also be fixed. This means that each parameter should cover a bounded one-dimensional domain, thus creating a design space with a dimension equal to the number of input parameters.

Figure 2.3a shows an example where two variables, each spread over a domain of $[0, 1]$, define a design space of $[0, 1]^2$.

2.3.2 Sampling

Sampling can be obtained by either traditional deterministic methods, such as the Central Composite Design (CCD), or stochastic methods such as the Latin Hypercube Sampling (LHS) methods.

2.3.2.1 Traditional deterministic methods

Adams et al. [2014] put together an overview of the most used deterministic methods summarised in this section.

Grid design is overlaying a grid over the design space and sampling the points from the grid (see Figure 2.2a). This is a fully factorial design method. In fact, a perfect grid is seldom used because it may take a lot of points to detect small but significant variations of the response surface. Instead, the grid is slightly modified with a random perturbation to easily detect certain variations. However, the random perturbation needs to be carefully set to guarantee detection of small variations.

CCD relies on a partial factorial design that chooses center points as initial samples and then sequentially adds "star points" or axial points to the initial group of samples (see Figure 2.2b). Axial points are added at a certain distance - the factor f of the case - outside the range of the design space until the curvature of the response surface is detected. This approach is particularly helpful for dynamic processes since it can build on the previous factorial experiment. However, depending on the choice of f and thus the expansion of the design space, the accuracy and the run-time of the sampling can vary significantly.

Box-Behnken Design (BBD) The sample points of a BBD are the center points of each edge in the domain of the design space (see Figure 2.2c). Because of the lack of the factorial design, BBD is more efficient than CCD; however, it does not allow for sequential experiments.

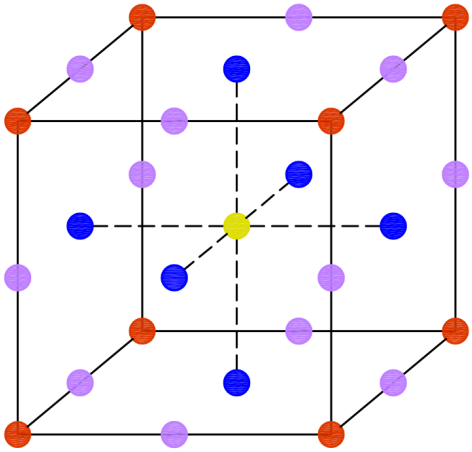

(a) Grid sampling requiring 27 samples for a unit cube design space

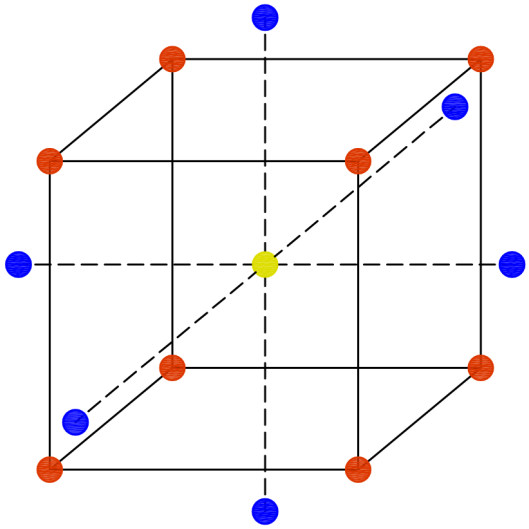

(b) CCD requiring 15 samples for a unit cube design space

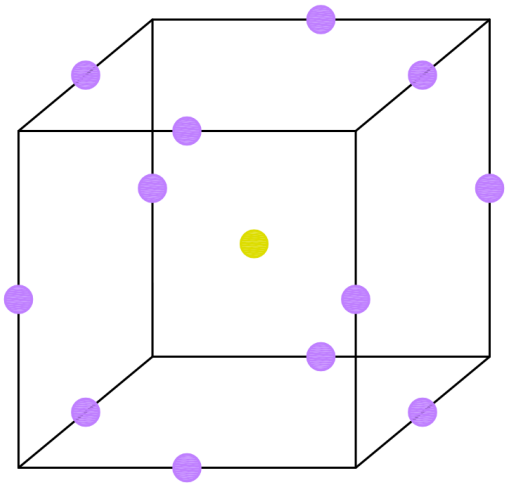

(c) BBD requiring 13 samples for a unit cube design space

Figure 2.2: Traditional sampling methods. source: [Bataleblu, 2019]

2.3.2.2 Stochastic methods

The Monte Carlo method is based on a random selection of points at which calculations will be carried out. This method is generally used as a reference because it does not require interpolation for the reconstruction of the response surface [Mouret, 2012]. However, its rate of convergence is proportional to the root of the number of points used. Therefore, The Monte Carlo method has a huge calculation cost. For instance, for a calculation with two uncertain parameters (input turbulence rate and turbulent Reynolds number) on a turbine blade, it takes 30,000 points to obtain the convergence for the prediction of the transition abscissa [Mouret, 2012]. This cost, thus, makes it difficult to use for various applications.

OA design Orthogonal Array (OA) sampling allows for systematic determination of the effect of variables/factors in the design space. An OA sample set is defined by four properties:

- number of samples m;
- number of input parameters n;
- number of symbols s - controls the level of stratification in sampling. A higher s increases stratification of samples and reduces replications;
- strength of the orthogonal array r - number of columns where all possibilities occur the same amount of times.

From these properties, the spread of samples can be maximised to guarantee a representative sample set of the design space. There are rules that control these properties. For instance, the number of samples m needs to be a multiple of r^2 to have a good sample set [Adams et al., 2014].

LHS In LHS, the domain is considered as a hypercube cut into subdomains of equal probabilities (see Figure 2.3). Sampling must have at least one point in each hyperplane. There are then different combi-

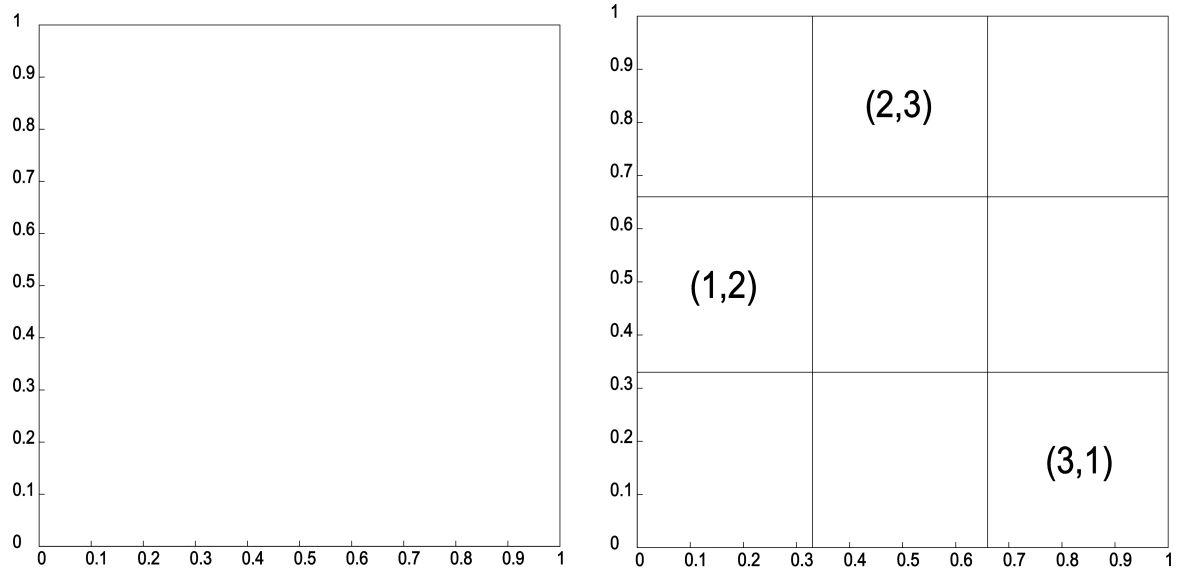

(a) Design space of $[0, 1]^2$

(b) LHS samples spread over the domain

Figure 2.3: LHS sampling over a domain. source: [Bataleblu, 2019]

nations of samples, which are explored until convergence. LHS tries to fulfill the following two requirements:

- Space-filling: the distance between two points must be as large as possible (see Figure 2.4);

- Independence between factors/variables: the determinant of the correlation matrix must be as large as possible.

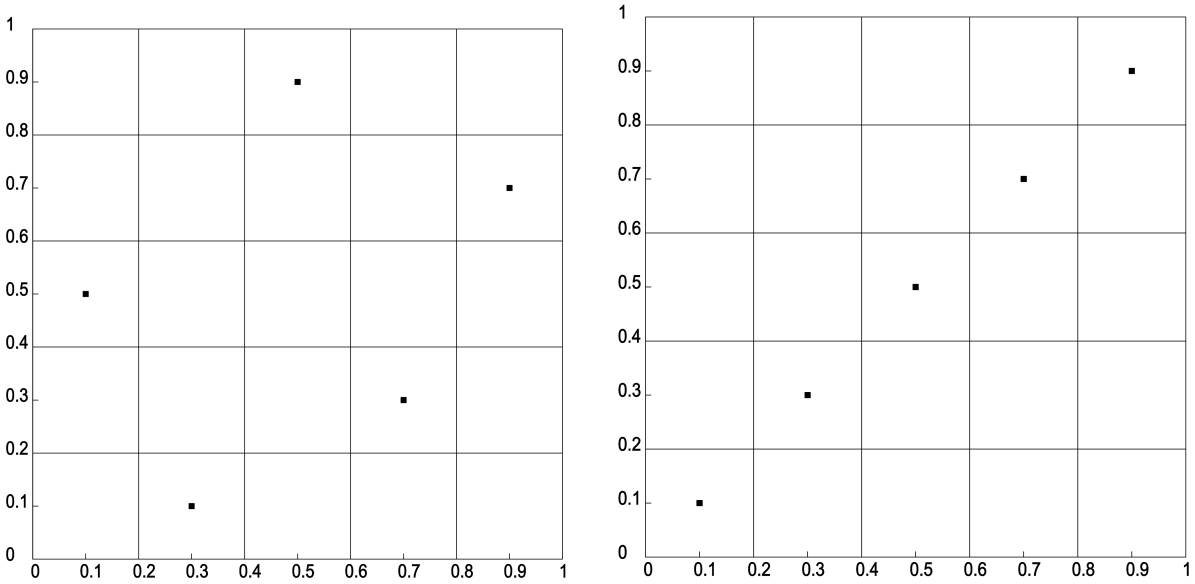

(a) Space-filling LHS samples

(b) Non-space-filling LHS samples

Figure 2.4: Space-filling samples. source: [Santer et al., 2018]

LHS is particularly useful for a large number of input parameters. To ensure the previous two requirements, Santer et al. [2018] suggest a rule-of-thumb depending on the number of input variables n to the analysis. The minimum number of samples required is $10n$. If no sensitivity is reached, the number of samples can be increased as follows: $20n$, $30n$, etc. until sensitivity is detected.

2.3.3 Evaluating samples depending on process

2.3.3.1 Sensitivity Analysis (SA)

SA consists of quantifying the influence of different parameters in the model over a response function. Thus, the analysis aims to determine whether an input parameter is "active" or not and how the parameter influences the output [Santer et al., 2018]. Therefore, after sampling the design space, the response function needs to be statistically evaluated. An ANalysis Of VAriance (ANOVA) is carried out to identify the effects of input variables on an output variable. ANOVA makes it possible to model a linear relationship between qualitative or quantitative factors and a quantitative response variable in order to identify the effects of the different factors. It creates groups from the combination of the different input variables; then, it uses F-tests to statistically test if the groups' means are equal. If the means are equal, there is no sensitivity to the factors. The higher the value of F, the higher the confidence to reject the null hypothesis that there is no sensitivity. The p-value in ANOVA indicates the confidence interval of the sensitivity. The lower the p-value, the more influential a factor is. A p-value lower than 0.05 means a confidence interval of 95%, whereas a p-value lower than 0.01 means a confidence interval of 99%. [Chen and Peng, 2013]

2.3.3.2 Surrogate model building

Surrogate models are an inexpensive approximation of a function that would otherwise take a long time to output an answer. The surrogate is defined by a certain number of samples depending on the sampling method chosen (see Section 2.3.2). Surrogates can be used for approximate interpolation of the design space or as an initial input for optimisation (See Section 2.4).

2.4 Optimisation

Mathematically speaking, optimisation is searching for an optimum of a function by manipulating a set of parameters. In PBD, optimisation is the search of the best solution that answers a design problem by transforming the question to a function that either needs to be minimised or maximised. The algorithms used for optimisation are generally based on a feedback-based loop. Some input is fed to a process that gives an output. That output is compared to the objective set. If the objective is reached, the optimisation stops; otherwise, the input is changed depending on the previous output; the process is repeated until the objective is reached, i.e.until convergence is reached.

2.4.1 Optimisation problem formulation

When optimising design solutions, it is important to correctly set up the optimisation to get relevant output. First, for the purpose of this study, the focus will be on a single-objective optimisation. A single-objective optimisation problem is defined by:

1. A design space: the set of domains defined by the different variables of the problem;
2. The objective function: defines the goal to be reached that needs to be minimised or maximised. There are two types of objective functions: a multimodal function with several optima (local and global); whereas, a unimodal function has only one minimum/maximum, the global optimum.
3. A set of constraints: a set of equalities or inequalities that the design space variables must satisfy. These constraints limit the search space.

Each point in the domain is one possible solution to the problem. Optimisation methods look for the point or the set of points in the design space that satisfy the set of constraints, and that maximise or minimise the objective function. It is very important to conduct a SA prior to the optimisation to not overload the optimisation with too many input parameters.

2.4.2 Optimisation methods

There are different methods and algorithms for optimisation, each having its advantages and limitations depending on the problem studied. There are two categories of optimisation methods: global and local. For this study, a global optimisation method is required and thus this section presents three main methods of global optimisation.

2.4.2.1 Deterministic methods

Deterministic methods were first introduced to accurately solve particular problems such as continuous and linear problems under linear constraints. The main quality of global deterministic methods is that they do not require a starting point. These methods allow to handle constraints well, unlike stochastic methods, and can be applied to mixed problems (real or integer variables). They ensure that the overall solution to the problem is obtained. At convergence, the output to the optimisation is the exact solution to the problem [Hachimi, 2013]. However, in design problems, the objective functions are seldom straightforward linear functions. This hinders the use of deterministic optimisation methods for design purposes.

2.4.2.2 Stochastic methods

Stochastic optimisation methods rely on probabilistic and random convergence mechanisms. These techniques can therefore give different results for the same initial setup. There are a number of stochastic optimisation methods; only two will be presented in this section.

Metaheuristic methods Metaheuristics are inspired by analogies with reality, such as physics (e.g.: simulated annealing), biology (e.g.: genetic algorithm), or ethology (e.g.: colonies of ants). Slower to converge than deterministic methods, metaheuristics have qualities to locate the global optima of complex problems without requiring knowledge of the derivatives of the objective function. They either accept a degradation of the objective function during their progression or use a population of points as a search method [Hachimi, 2013]. A large number of metaheuristic methods exist and their advantages and disadvantages depend on the application. The following will only introduce two of the most used algorithms for CFD-related optimisation:

- A GA, also called evolutionary algorithm, is inspired by the concept of natural selection proposed by Charles Darwin. The technical terms used are a direct mapping to the vocabulary of the theory of evolution and genetics. Therefore, GA includes individuals (potential solutions), populations, genes (variables), chromosomes, parents, descendants, reproductions, etc [Hachimi, 2013]. The individuals that would form a population are the points in the design space and their adaptation is the function to be optimised. These algorithms change a population iteratively. Some individuals reproduce and their genes are kept in the gene pool. Others mutate or even disappear. Only the best-adapted individuals are expected to survive. It is assumed that genetic inheritance of generations evolves the population to become better adapted to its environment and by analogy to better respond to the optimisation criterion [Hachimi, 2013]. The main steps of a GA are:
  - Step 1: Generation of the initial population;
  - Step 2: Constitution of a new population:
    * Measurement of the adaptation of each individual;
    * Reproduction of individuals according to their adaptation. The most efficient ones reproduce first;
    * Crossing of pairs of randomly chosen sequences;
    * Mutation of sequences drawn at random.
  - Step 3: Stop criterion - It can be defined according to the output, the number of generation, adaptation of the best individual, etc. (see Figure 2.5)
- Ant Colony Optimisation (ACO) is a probabilistic technique to optimise a problem. The ant colony method is based on the social behavior of some insects, such as ants, to solve path-finding problems. This behavior is possible because ants communicate with each other indirectly by depositing chemicals, called pheromones, on the ground. This type of indirect communication is called stigmergy [Hachimi, 2013]. The concept is the longer the path between the nest (origin) and a food source (destination), the lower the pheromone levels on that path because the chemical evaporates with time. This means that the pheromone level is higher on the shortest path and eventually attracts more ants towards it, again increasing the pheromone levels on that shortest path. Therefore, the shortest path is more likely to be taken by ants than the other paths, and will eventually be taken by all ants [Martinez et al., 2008]. In ACO, a graph is constructed from vertices (possible solutions) and edges connecting those vertices. Artificial ants travel that graph iteratively and updates the vertices and edges with the quality of the solution (the pheromone). At each iteration, new ants will be drawn to higher quality paths, while updating the vertices and edges of the graph, until they all converge to one path and one vertex which is the solution to the problem [Martinez et al., 2008].

The quality of the results and the time-cost of each of these algorithms depend on the case to be optimised and how each algorithm is implemented.

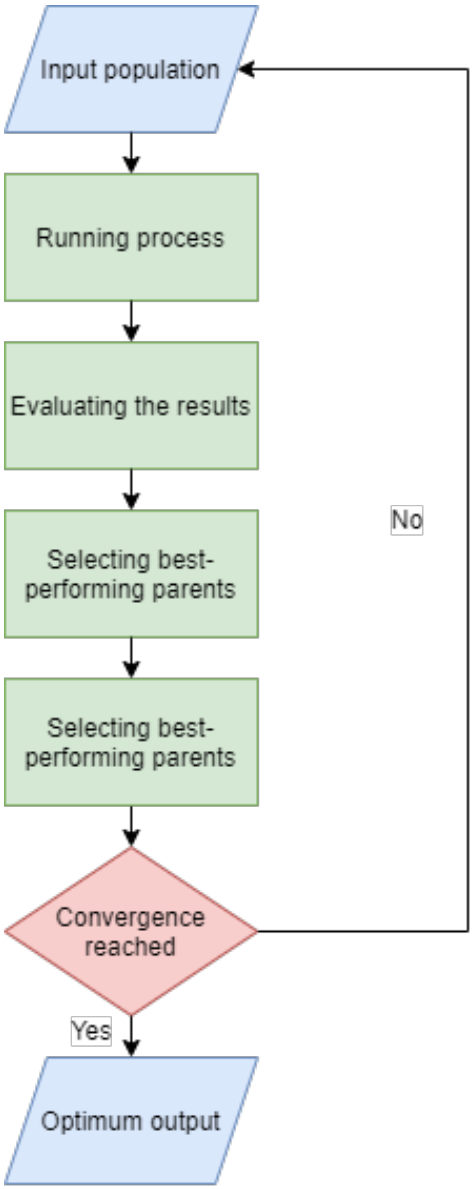

Figure 2.5: Flowchart of GA

Surrogate-Based Optimisation (SBO) SBO is a stochastic optimisation method that differs from the previous deterministic and stochastic methods. This method was primarily developed to lower the cost of metaheuristic algorithms. Instead of using a time-expensive objective function over the whole design space, it adopts a surrogate model defined by the same design space as the objective function. The surrogate model is created by carefully chosen sample points that are later fitted into a response surface using interpolation [Estrado, 2019]. For global optimisation methods, Polynomial Regression, Kriging, and Radial Basis Function (RBF) are common interpolation methods to create the response surface. The response surface is updated during optimisation in case this is needed. There are, however, different hybrid ways to conduct a surrogate-based optimisation. Hachimi [2013] and Casella [2020] present approaches that combine different metaheuristic optimisation both local and global to reach an optimum. For instance, global metaheuristic optimisation can be conducted for a limited number of generations. The result is used as the surrogate to run a local metaheuristic optimisation in regions of interest. Another approach is to build a surrogate using DACE methods and using it to run a global metaheuristic optimisation [Santer et al., 2018]. Figure 2.6 shows the general steps of a SBO.

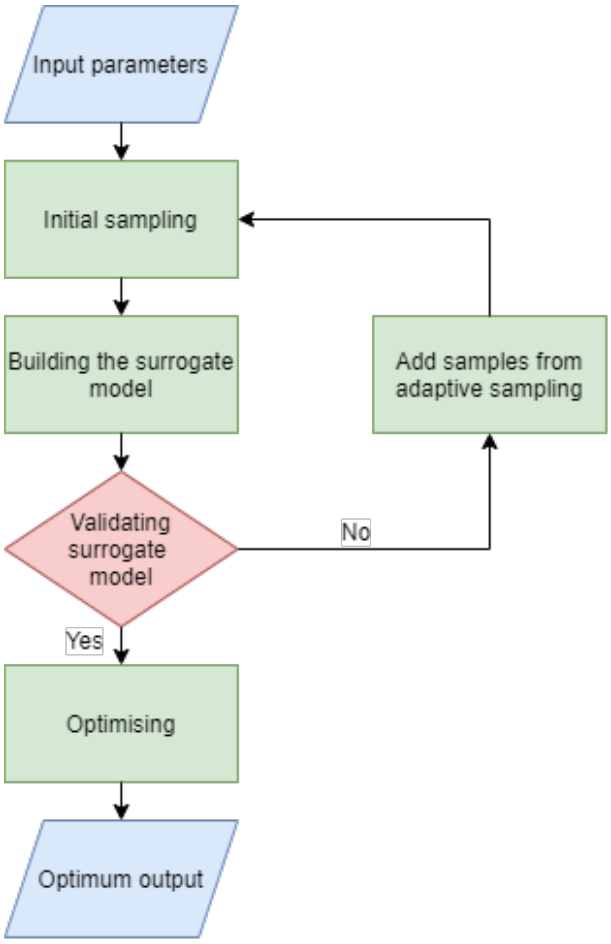

Figure 2.6: Flowchart of SBO

3 Methodology

This chapter introduces the steps taken in this study. It also introduces the area of study and some dunes vocabulary that will be used in later sections. Then, it details all the steps taken during the research that concludes in an optimal solution for the problem.

3.1 Research workflow

Based on chapter 2, Figure 3.1 summarises the steps that this study follows and their outcome. The workflow starts with input parameters that affect the dunes formation. These parameters need to be filtered by identifying the most influential variables with SA from the DACE. The most influential parameters are then fed to an optimisation algorithm that checks for the sediment mobility until convergence. Both the DACE and the optimisation run CFD simulations in order to get their objective response.

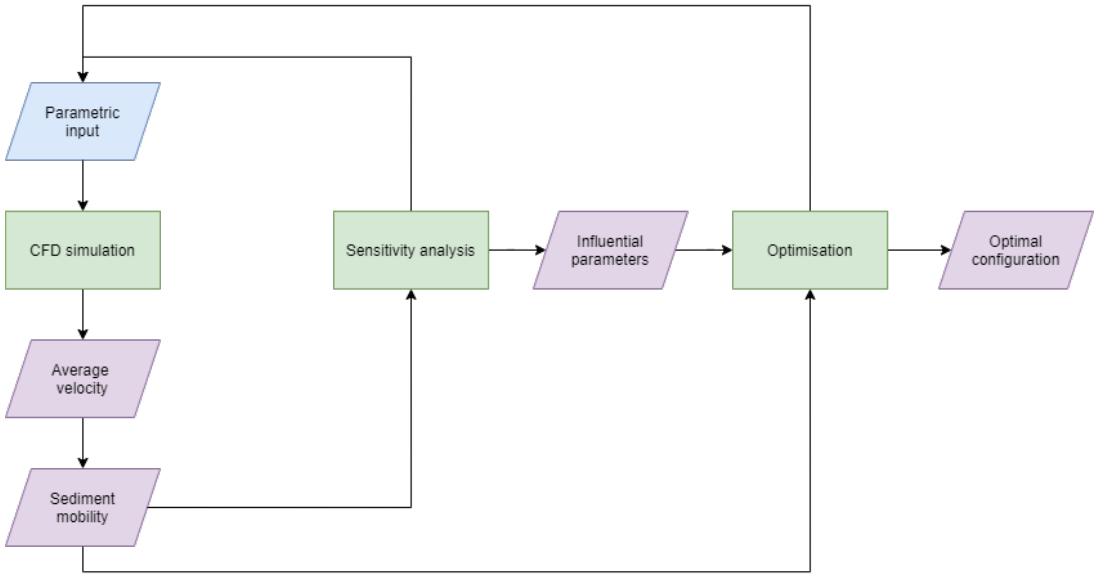

Figure 3.1: Research workflow

3.2 Study area

Being part of the ShoreScape project, the reference coast is in Noordwijk as it is perceived as a typical Dutch coastline from the point of view of orientation and wind climate. For this model, it is assumed that the coast is defined with straight lines. A typical cross-section of the coast is given in figure 3.2.

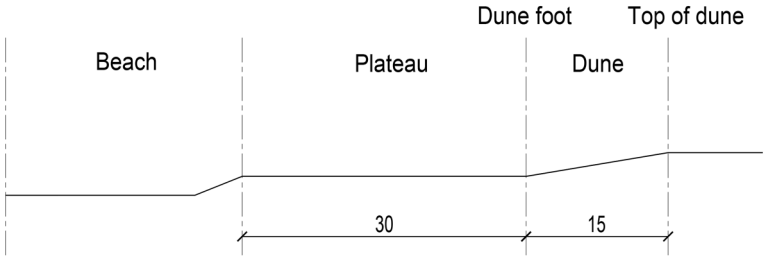

Figure 3.2: Typical coast cross-section showing the plateau and the dunes relatively to the beach. The dimensions of the plateau and the dunes are assumed to be constants and are in meter

3.3 Parametric input

3.3.1 Defining the parameters

There are two types of parameters that affect the formation of dunes: geometric parameters related to the houses individually and to the configuration as a whole, and wind properties parameters. Each type of these parameters includes two categories: constant and variable parameters. The choice of each category for a given parameter is presented in this section and is based on the previous work done in this field (See [van Bergen et al., 2021; van Onselen, 2018]). This section introduces these parameters and explains how each variable parameter was implemented in the model.

3.3.1.1 Parametric geometry

First, the beach houses have standard dimensions and are modelled as straight boxes and thus their geometry is defined by three constant parameters:

- Length of house: $L = 7$ m;
- Width of house: $l = 3$ m;
- Height of house: $h = 3$ m.

In addition, each beach house is rotated relatively to the shoreline, thus defining the first variable parameter angle α such as $0° \leq \alpha \leq 90°$. This interval allows to test the impact of wind-facing gaps on widening of the dunes.

Second, a configuration includes five beach houses and is defined by one constant parameter and two variables:

- Inter-distance between houses - $d = 3$ m;
- Rotation angle relative to the shoreline - $0° \leq \beta \leq 90°$;
- Distance to the foot of the dunes - 1 m $\leq dd \leq$ 10 m.

The choice of d is based on van Onselen [2018] where an inter-distance of 3 m allows the smallest reverse flow area. The interval of β is chosen to maximise the wind-facing surface. The interval of dd is chosen in a way to allow enough rotation of the configuration on the plateau.

In conclusion, three geometric parameters define the design space. The following explains the ambiguities of each parameter and how they were implemented.

Angle of individual houses to shoreline - α Even though α is a parameter specific to the houses and not to the entire configuration, the latter is greatly affected by α (see Figure 3.3). Since the configuration needs to respect the 3 m inter-distance, a large alpha value causes the configuration to expand in an unfeasible manner (see Figure 3.4). Consequently, the definition of the 3 m inter-distance shifts when alpha is larger than 70°. Instead of measuring 3 m between the larger sides of the houses, after the 70° angle, the 3 m is measured between the shorter sides of the house (see Figure 3.3c). The 70° choice is to maintain four initially proposed configurations.

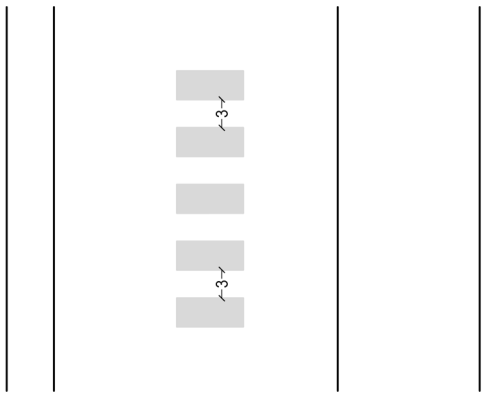

(a) Configuration: α = 0°; β = 0°; dd = 10 m

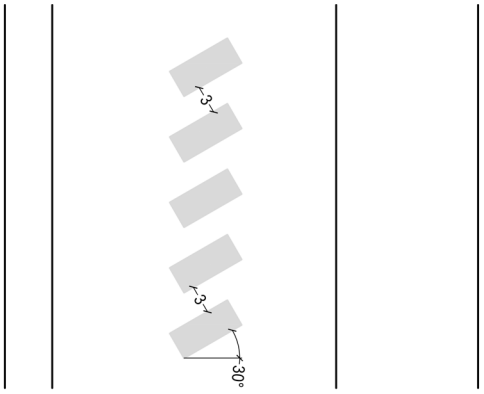

(b) Configuration: α = 30°; β = 0°; dd = 10 m

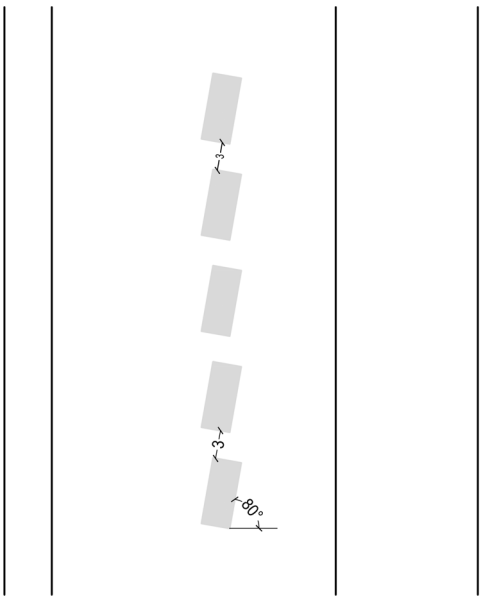

(c) Configuration: α = 80°; β = 0°; dd = 10 m; with inter-distance shifting after 70°

Figure 3.3: How the geometry of the configuration changes with α

Angle of entire configuration to shoreline - β Rotating the configuration has to ensure that the configuration stays within the plateau. For this reason, for each configuration, β is multiplied by a ratio r_β computed as follows:

$$r_\beta = \frac{a_{\max}}{90} \tag{3.1}$$

where $a_{\max}$ is the maximum angle in degrees that the configuration can rotate without surpassing the plateau. This angle also factors in a small setback from the plateau limit (see Figure 3.5).

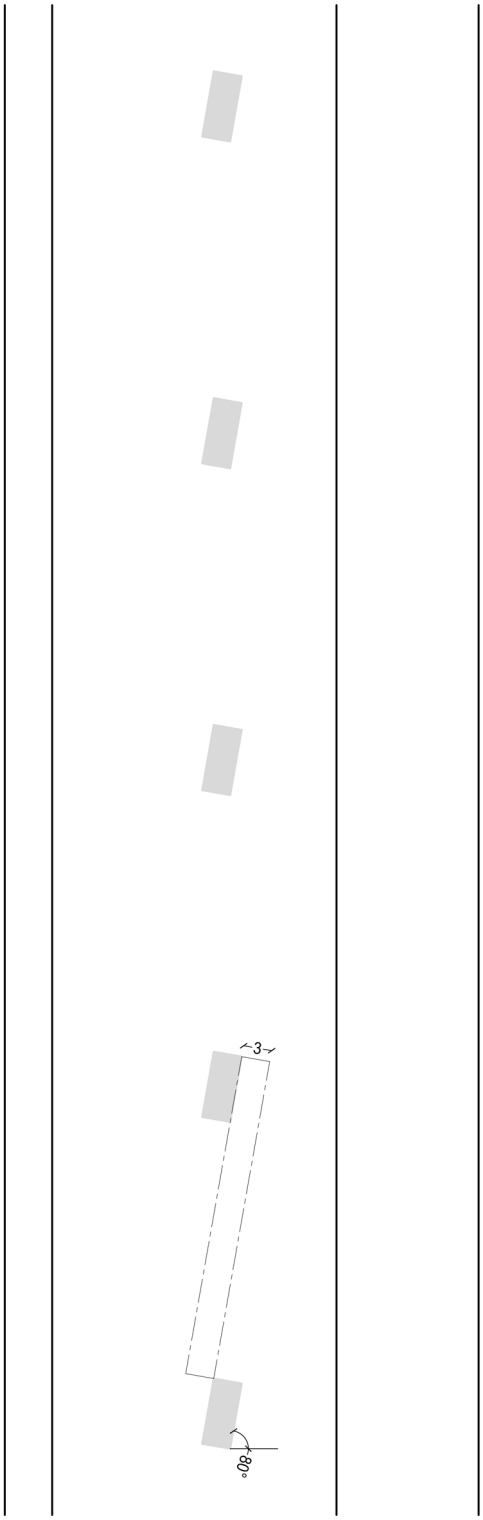

Figure 3.4: Configuration: α = 80°; β = 0°; dd = 10 m; with inter-distance not shifting after 70°

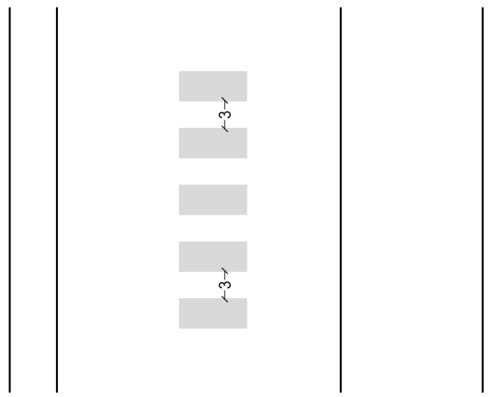

(a) Configuration: $\alpha = 0°$; $\beta = 0°$; $dd = 10$ m

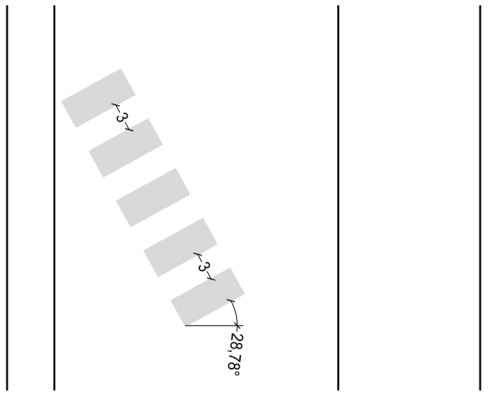

(b) Configuration: $\alpha = 0°$; $\beta = 90°$; $dd = 10$ m; with r_β

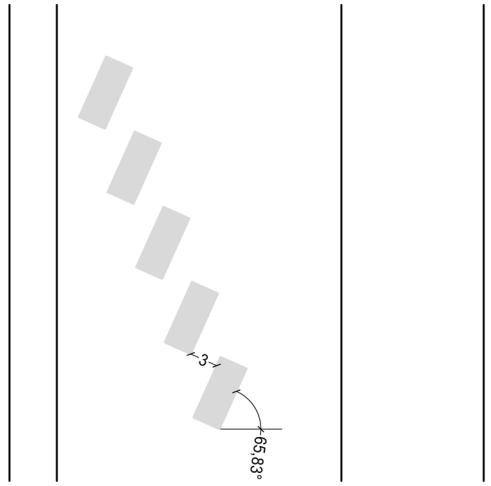

(c) Configuration: $\alpha = 45°$; $\beta = 90°$; $dd = 10$ m; with r_β

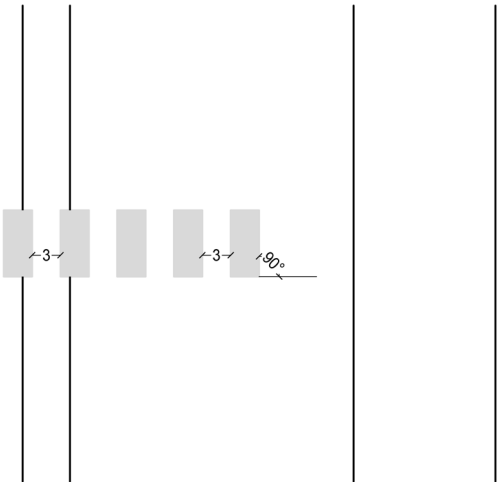

(d) Configuration: $\alpha = 0°$; $\beta = 90°$; $dd = 10$ m; without r_β - some houses are either completely or partially outside the plateau

Figure 3.5: How the geometry of the configuration changes with β

Distance of configuration to dunes - *dd* For determining how far away the configuration should be especially for a rotated one, the bounding box of the configuration is determined and used as a reference to place it relative to the dunes (see Figure 3.6).

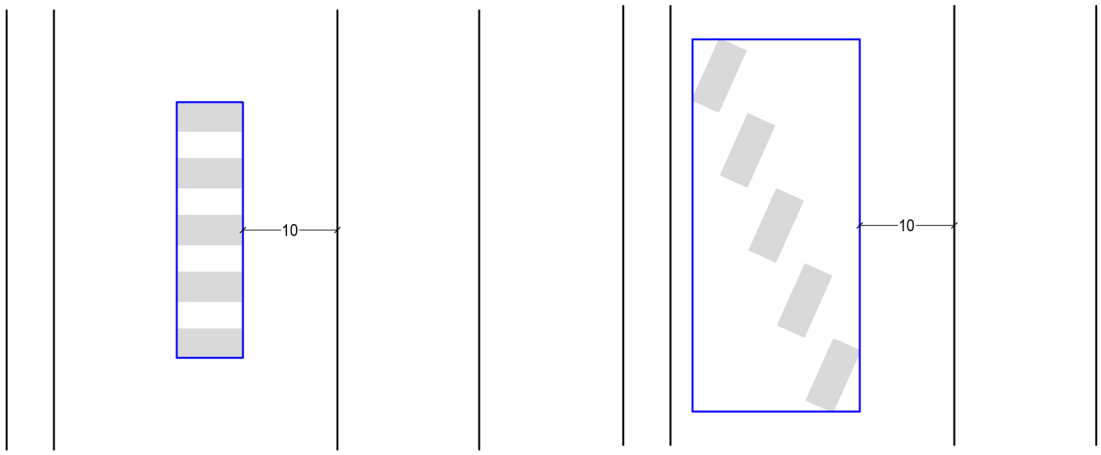

(a) Configuration: $\alpha = 0°$; $\beta = 0°$; $dd = 10$ m (b) Configuration: $\alpha = 45°$; $\beta = 90°$; $dd = 10$ m

Figure 3.6: How the geometry of the configuration changes with *dd* - blue rectangle = bounding box

3.3.1.2 Wind properties

Two main wind properties affect the formation of dunes: wind speed and wind direction. For wind speed, the average speed from the wind rose at Noordwijk is used. As for wind direction w, it was decided to run all the configurations with a dominant wind direction, 60°. In the end, the chosen optimal solution will run with 12 wind directions, each given a weight depending on occurrence percentage from Figure 3.7. This can approximate the relative difference between accounting for one dominant direction and accounting for twelve weighted directions.

3.3.2 Generating the input geometry

To generate the geometry, Grasshopper was first used to easily visualise how each parameter is changing the geometry. However, the Grasshopper script was later translated into OpenFOAM's geometry transformation language, reducing software coupling to avoid cross-platform problems. Other than the geometric variables, six STL files, five STL files for 5 houses and 1 STL file for terrain at the initial position, are also needed. The initial state is shown in Figure 3.8. The main steps, regardless of the software, are shown in the pseudo-code 3.1.

3.4 CFD

This study will mainly focus on the numeric approach to wind studies. Since CFD simulations support 3D models, CFD was chosen over LGCA.

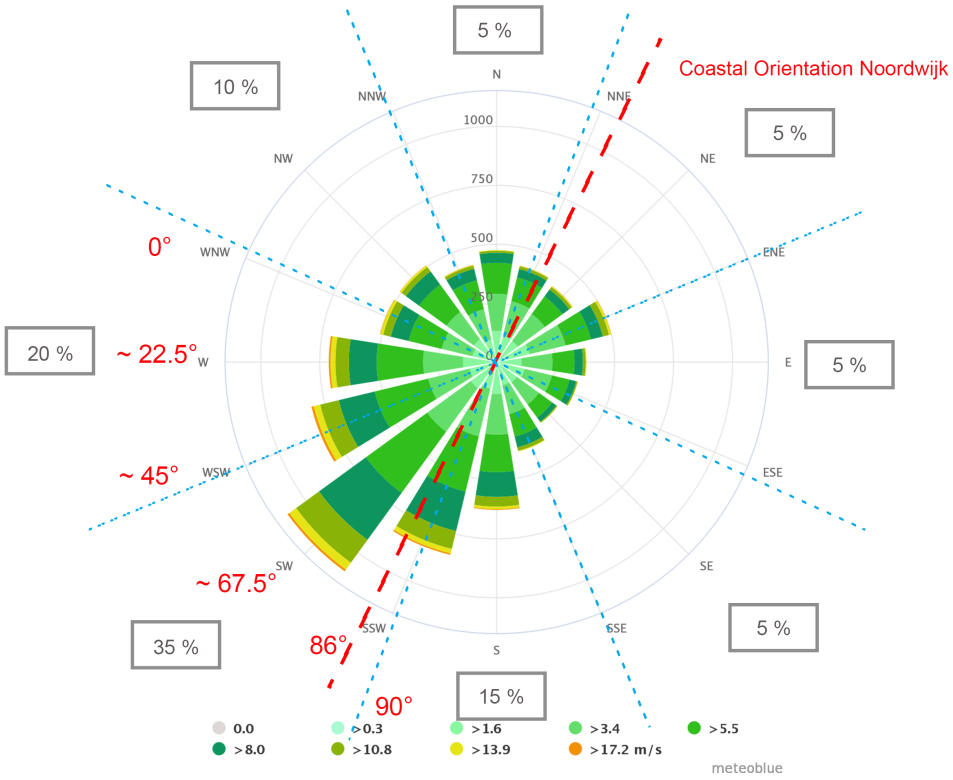

Figure 3.7: Wind direction occurrence. Source: [van Bergen et al., 2021]

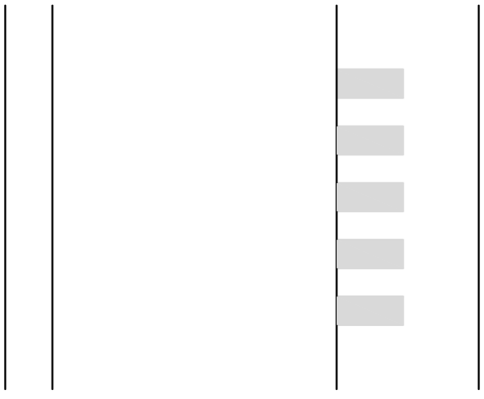

Figure 3.8: Initial state of configuration before generating the input geometry for the automated runs

Algorithm 3.1: Generate input geometry

Input: α, β, dd, houses files hh_i, terrain file t
Output: changed configuration F

if $\alpha \leq 70$ **then**
  for $i \leftarrow 0$ **to** 5 **do**
    $hh_i \leftarrow$ rotate hh_i by α;
    $hh_i \leftarrow$ translate hh_i by a distance d_{70} to maintain the 3 m between the large sides of the houses;
else
  for $i \leftarrow 0$ **to** 5 **do**
    $hh_i \leftarrow$ rotate hh_i by α;
    $hh_i \leftarrow$ translate hh_i by a distance d_{90} to maintain the 3m between the shorter sides of the houses;
$hh \leftarrow$ combine all hh_i as one entity;
$hh \leftarrow$ rotate hh by β*r_β;
$bbox \leftarrow$ get bounding box of hh;
$xmin \leftarrow$ get minimum x from $bbox$;
$xmax \leftarrow$ get maximum x from $bbox$;
$ymin \leftarrow$ get minimum y from $bbox$;
$xtotal \leftarrow$ $xmax$-$xmin$;
$hh \leftarrow$ translate hh by vector (-$xmin$, -$ymin$, 0);
$hh \leftarrow$ translate t by vector ($xtotal$ + dd, 0, 0);
$F \leftarrow$ combine hh and t;

3.4.1 Governing equations and discretisation schemes

For this study, the RANS - RNG k-ϵ model will be used since RANS is the most time-efficient model and RNG k-ϵ is the most suited for the built environment. The governing equations for RANS are:

$$\frac{\partial \overline{u_j}}{\partial x_j} = 0 \tag{3.2}$$

$$\overline{u_j}\frac{\partial \overline{u_i}}{\partial x_j} = -\frac{1}{\rho}\frac{\partial \overline{p}}{\partial x_i} + \nu\frac{\partial^2 \overline{u_i}}{\partial x_j \partial x_j} - \frac{1}{\rho}\frac{\partial \overline{u_i' u_j'}}{\partial x_j} \tag{3.3}$$

where $\overline{u_i}$ is the time-averaged velocity components, r is the density, p the pressure, ν the kinematic viscosity and $\overline{u_i' u_j'}$ the specific Reynolds stress tensor [García-Sánchez et al., 2014]. As for the equations for the RNG k-ϵ model, the k and ϵ equations, where buoyancy is neglected, are given below [CFDOnline, 2010]:

$$\frac{\partial}{\partial t}(\rho k) + \frac{\partial}{\partial x_i}(\rho k u_i) = \frac{\partial}{\partial x_j}\left[\left(\mu + \frac{\mu_t}{\sigma_k}\right)\frac{\partial k}{\partial x_j}\right] + P_k - \rho\epsilon \tag{3.4}$$

$$\frac{\partial}{\partial t}(\rho \epsilon) + \frac{\partial}{\partial x_i}(\rho \epsilon u_i) = \frac{\partial}{\partial x_j}\left[\left(\mu + \frac{\mu_t}{\sigma_\epsilon}\right)\frac{\partial \epsilon}{\partial x_j}\right] + C_{1\epsilon}\frac{\epsilon}{k}P_k - C_{2\epsilon}^{*}\rho\frac{\epsilon^2}{k} \tag{3.5}$$

where

$$C_{2\epsilon}^{*} = C_{2\epsilon} + \frac{C_\mu \eta^3 (1 - \eta/\eta_0)}{1 + \beta\eta^3} \tag{3.6}$$

and

$$\eta = Sk/\epsilon \tag{3.7}$$

and

$$S = (2S_{ij}S_{ij})^{1/2} \tag{3.8}$$

The calculations do not take into consideration moisture and humidity.

A basic case shown in Figure 3.3a was set up to validate the computational model (see Section 3.4.3). The basic case has a the following dimensions: $\alpha = 0°$; $\beta = 0°$; $dd = 10$ m. Using the SIMPLE algorithm, the initial simulations for the basic case were run for 5000 iterations to ensure residuals convergence. Second-order upwind discretisation scheme was chosen for the velocity divergence and linear interpolation scheme for gradient calculation. However, all the runs used for the DACE and the optimisation are set to 3000 iterations.

3.4.2 Boundary conditions

Boundary conditions are the initial estimates of field values. For the inlet boundary conditions, the following equations to get the profiles for velocity, turbulence kinetic energy and dissipation were used:

$$U = \frac{u_*}{\kappa} \ln(\frac{z + z_0}{z_0}) \tag{3.9}$$

$$k = \frac{u_*^2}{\sqrt{C_\mu}} \tag{3.10}$$

$$\epsilon = \frac{u_*^3}{\kappa(z + z_0)} \tag{3.11}$$

where κ is the von Karman constant equal to 0.41. The roughness length z_0 is equal to 0.0005 m which is corresponding to the sand roughness length [Hesp and Smyth, 2019]. For the reference wind speed U, the average wind speed from the wind rose is used and set to 4.9 m s^{-1}. The friction velocity is deduced from equation 3.9 using the specified z_0 and U.

Two different wall functions are used for the houses and the terrain to account for the law of the wall. A standard wall function is used near the houses' wall boundary; whereas, a modified wall function that models the ABL close to the terrain is used for the terrain boundary [Parente et al., 2011].

3.4.3 Set up of the computational model

The computational model follows the best practice guidelines proposed in Blocken [2015] to ensure accurate and reliable CFD simulations.

3.4.3.1 Computational domain dimensions

The computational model is a closed domain that approximates the real-life physical model. However, in reality, there are no boundaries for the wind other than the terrain (ground and buildings) surface. This means that all the fields near the other boundaries of the model are not 'real' values and thus those

boundaries need to be placed far enough from the studied area to not introduce erroneous results. To avoid this problem, there are two directional blockage ratio conditions that need to be met.

$$BR_L = L_{\text{building}} / L_{\text{domain}} \leq 17\% \tag{3.12}$$

$$BR_H = H_{\text{building}} / H_{\text{domain}} \leq 17\% \tag{3.13}$$

Where L_{building} is the dimension of the built area in the windward direction; L_{domain} is the dimension of the domain in the windward direction; H_{building} is the height dimension of the built area; and H_{domain} is the height dimension of the domain. Since different configurations will be tested automatically and to ensure consistency between simulations, the computational domain has an all-inclusive geometry which means that its dimensions are suited for all configurations. The resulting domain is a rectangular box with the following dimensions: x = 205 m; y = 330 m; z = 81 m.

3.4.3.2 Computational mesh

Meshing the domain is an important step to ensure the validity of the results. CfMesh was used to generate the mesh. The background cell size is 1.8 m with two refinement boxes. One big refinement box with a 0.6 m cell size ensures a smooth transition between the large background cells and the small cells around the areas of interest. The areas of interest with a 0.15 m cell size are the five houses and the terrain area from the houses to the top of the dunes in the direction of the wind (see Figure 3.9 and 3.10a). Additional refinement is added near the terrain surface.

There are two ways to check that the mesh will generate valid results: mesh independence and residuals convergence. The fields sampled for these checks are the velocity in the x-direction U_x, in the y-direction U_y, and in the z-direction U_z, the pressure p, and the turbulence fields k and ϵ. Both checks were first tested against the basic case (see Figure 3.3a) and then random samples were checked to make sure that the change in the configuration does not affect the validity of the mesh.

Mesh independence checks whether a change in the resolution affects the results. For this case, three meshes are generated: coarse, medium, fine. A constant ratio of 1.5 between the cell sizes of consecutive meshes is used. Thirty probes were placed in front of the houses for the check. When plotting the values at the probes for each mesh resolution, the medium mesh values should be closer to the values of the fine mesh to validate the mesh. Other than plotting the results of the probes, three error values are computed based on [Celik et al., 2008]: the approximate relative error e_a^{21}, the extrapolated relative error e_{ext}^{21}, and the fine-grid convergence index GCI_{ext}^{21}. The lower these values are the better. For this study, error values less or equal to 5% are accepted. The median of these values is computed to avoid outlier sensitivity.

Residuals convergence checks that the change in fields' values between iterations is either very small or equal to zero. There are two ways to check for residuals convergence:

- Plot residuals and check that the graph plateaus at the end;
- Check that the relative difference between the values of the last iterations is under a certain threshold. For this study, a threshold of 10^{-4} is used.

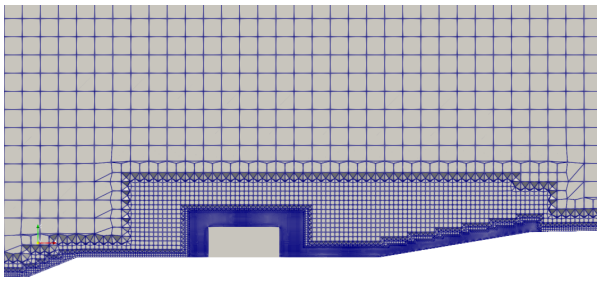

(a) Cross-section view of mesh showing the three cell sizes and the extra refinement for the terrain

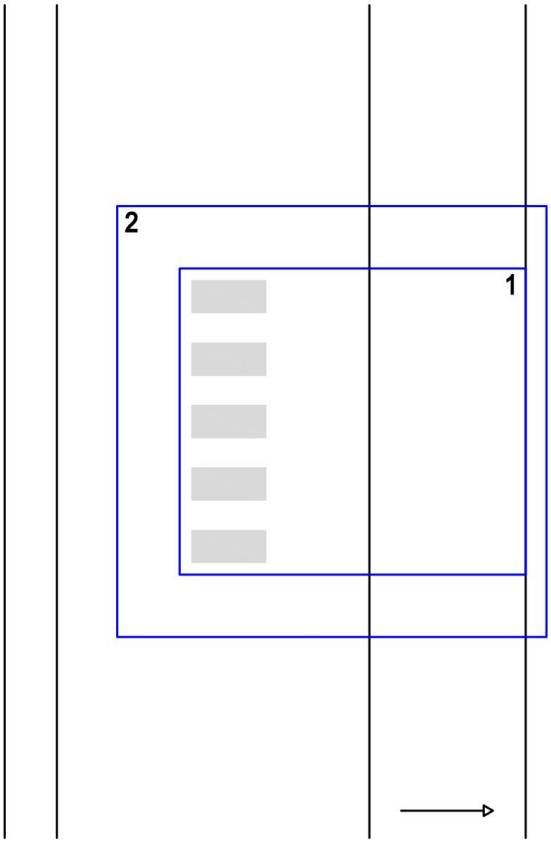

(b) Top view of the refinement areas. 1 = refinement area with 0.15 m cell size; 2 = big refinement box with a 0.6 m cell size; arrow is the direction of the wind

Figure 3.9: Mesh of basic case with $w = 0°$ showing the refinement levels

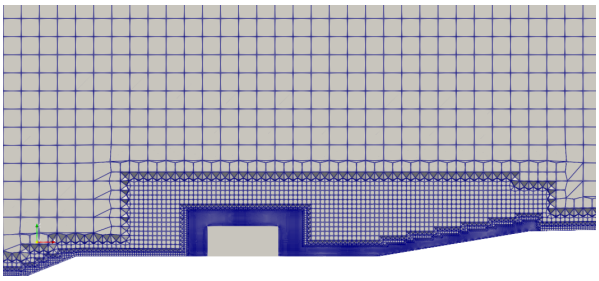

(a) Cross-section view of mesh showing the three cell sizes and the extra refinement for the terrain

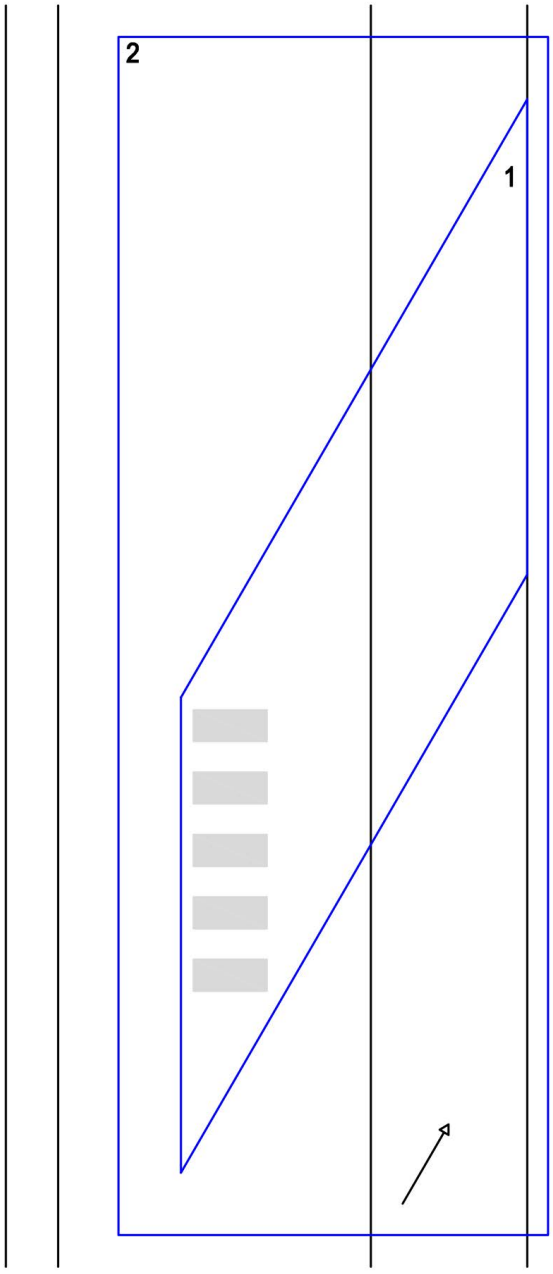

(b) Top view of the refinement areas. 1 = refinement area with 0.15 m cell size; 2 = big refinement box with a 0.6 m cell size; arrow is the direction of the wind

Figure 3.10: Mesh of basic case with $w = 60°$ showing the refinement levels

3.5 Sediment mobility

The aim of this thesis is to promote widening of dunes which is defined as the horizontal expansion of dunes in the direction of the beach (see Figure 3.11a). To quantify the sediment mobility, the line method discussed in Delgado-Fernandez [2011] has been adapted for this thesis. Two lines will be sampled for the field velocity: one at the beginning of the plateau (L1) and one at the foot of the dune (L2) (see Figure 3.11). Line 3 (L3) can be implemented to detect heightening of the dunes.

As mentioned in Section 2.2, sediment mobility is best measured at a maximum height of 50 cm. For this reason, the Shorescape project adopts a reference measuring height of 10% of the height of the houses studied. In this case, with houses of 3 m height, both lines are, thus, sampled at 30 cm over the plateau. The average transport rate at each line is then computed based on a simplified transport rate equation proposed by Delgado-Fernandez [2011]:

$$q_n = 1.16 \times 10^{-5} \times U^3 \cos\theta \tag{3.14}$$

where q_n is potential transport rate in $\mathrm{kg\,m^{-1}\,s^{-1}}$, U is wind speed in $\mathrm{m\,s^{-1}}$ and θ is angle of wind approach from shore perpendicular in degrees. Then, the transport rate from L1 is subtracted from L2. If the transport rate difference q is negative, it means there is sedimentation and, consequently, widening of dunes; otherwise, there is mobility.

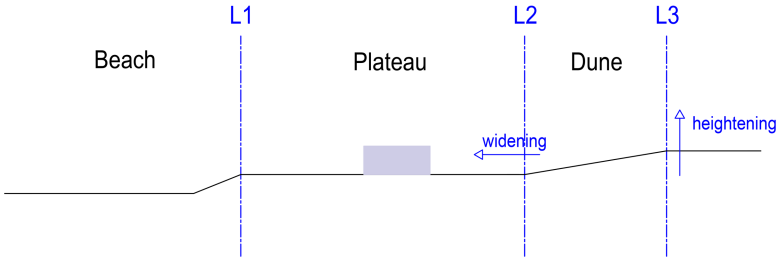

(a) Cross-section showing the widening and heightening of dunes with respect to L1, L2 and L3

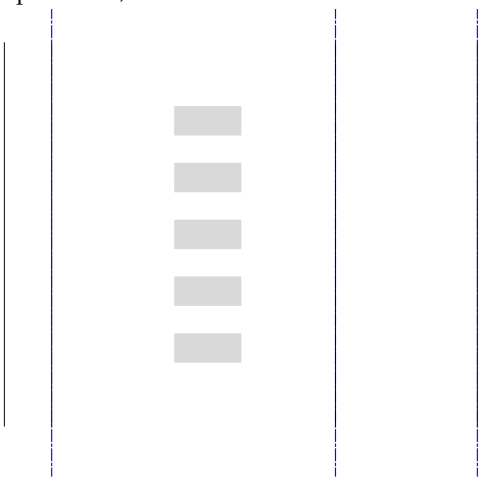

(b) Plan view of dunes with L1, L2 and L3

Figure 3.11: Lines used for sediment mobility quantification

3.6 DACE

For the DACE, the DAKOTA software was used coupled with OpenFOAM.

3.6.1 SA

To set up DAKOTA for the SA, the design space, the sampling method, and the response function need to be defined.

3.6.1.1 The design space

The SA will run a 3D design space defined with the three geometric variables:

- $0° \leq \alpha \leq 90°$;
- $0° \leq \beta \leq 90°$;
- $1\text{ m} \leq dd \leq 10\text{ m}$.

3.6.1.2 LHS-OA sampling

DAKOTA presents the option of conducting a LHS-OA sampling that combines the advantages of both sampling methods discussed in Section 2.3.2. It is a stochastic method that ensures stratified and space-filling samples to determine the main effects of the variables used. As for choosing the number of samples, the OA rule in Section 2.3.2.2 and the LHS rule in Section 2.3.2.2 need to be respected. The LHS rule requires samples ten times the number of input variables which is equal to 30. However, the OA rule requires samples with the square of the symbol, and the larger the symbol the better. Therefore, a symbol value of 7 is chosen and 49 samples will be generated, keeping a low number of samples while increasing stratification and respecting all the rules. It should be noted that, in theory, a symbol value of 6 could be used since 36 samples is enough to respect all the rules; however, DAKOTA only allows a prime number or 4 as a symbol value.

3.6.1.3 Objective function - Sediment mobility

The SA will use the approach proposed in Section 3.5 to detect the sensitivity of the parameters with regards to the horizontal expansion of the dunes. As mentioned in Section 2.3.3.1, the final result is an ANOVA with p-values indicating the sensitivity. A 95% confidence interval is the most commonly used interval to identify the influential parameters and will also be used in this study.

3.6.2 Surrogate model building

A "cheap" surrogate model, using a low number of samples, was built to try to predict the optimum before running the optimisation.

3.6.2.1 The design space

The SA results will define which parameters will qualify for the surrogate's design space.

3.6.2.2 LHS sampling

Since the parameter's effects is no longer needed at this point and it does require some extra time, it was decided not to use the OA sampling for building the surrogate. LHS sampling alone is adopted to generate representative sample points of the design space. For building the surrogate, some studies argue that the minimum sample size (10 times the number of input variables) presented in the LHS rules in Section 2.3.2.2 is not enough for a good surrogate model. Forrester et al. [2008] mention an approach that defines a number of representative points p for each input variable and not for the entire domain. This means that, if each input variable is represented by p points and there are n input variables, the number of samples should be p^n. The choice of p depends on the accuracy needed from the model. For this study, it has been decided to choose 10 points per input variable to approximate the design space.

3.6.2.3 Objective function - Sediment mobility

The response function for the surrogate model is the same sediment mobility as in Section 3.5. However, instead of using the response for ANOVA, first, it will be fitted into a response surface by using different interpolation techniques to predict the optimum. The response surface will be interpolated with a grid of cell size equal to 1°. Second, the response model will be passed as input for a surrogate-based optimisation.

3.7 Optimisation

DAKOTA does not guarantee convergence with the optimisation method chosen for this thesis. For this reason, the samples generated for this purpose will be used to quantify the relative error of the surrogate model discussed in Section 3.6.2.

3.7.1 The design space

The optimisation's design space is inherited from the surrogate model in Section 3.6.2.

3.7.2 SBO

Deterministic methods are not an option since the objective function is complex. Metaheuristic algorithms take, however, a longer time to converge. Therefore, a surrogate-based optimisation is the most suitable choice for this study. The surrogate will then be the input to a GA. A GA was chosen over an ACO because it is more commonly used for CFD-related optimisation and it is easier to implement in DAKOTA than an ACO. Based on the literature review in Casella [2020], the interpolation method should be Kriging and the initial population size of the GA should be $50n$ where n is the number of input variables. In this case, the initial population is set to 100. The mutation factor is set to 0.01 based on Schaffer et al. [1989] and DeJong [1975], a value that is not too high as to delay convergence nor too low as to loose potential combinations. In case the optimisation does not converge, the initial surrogate and the first generation will be used to approximate the trend and the optimum and to quantify the degree of error of the surrogate.

3.7.3 Objective function - Sediment mobility

The optimisation will minimise the transport rate difference to get the largest decline in rate between L1 and L2 (see Section 3.5). The convergence criterion is set as maintaining a change rate lower than 0.05% in the objective function over 3 generations.

4 Results and discussion

This chapter will present the verification results of the mesh used in this study. Afterward, it will go over the sensitivity analysis results and deduce the influential parameters to use for trend detection and optimisation. Finally, it will present the results from the surrogate and the first generation of the GA, explain the trends observed from the response functions, and conclude on design criteria for an optimum design approach for widening the dunes.

4.1 Mesh verification

Based on Section 3.4.3.2, after running the basic case and a few other samples, the mesh choice needs to be verified.

4.1.1 Mesh independence

Table 4.1 presents the three generated meshes and their resulting sizes. This table shows that the change in cell size, the 1.5 ratio, does not mean a 1.5 times change in cell count. In fact, the change in cell count between the consecutive resolutions is almost twice the cell count. This highlights the importance of the mesh independence to motivate the use of a certain mesh resolution.

Mesh	Cell size	Mesh size
Coarse	Background cell: 2.7 m Big refinement box: 0.9 m Small refinement areas: 0.23 m	2611652 cells
Medium	Background cell: 1.8 m Big refinement box: 0.6 m Small refinement areas: 0.15 m	6127361 cells
Fine	Background cell: 1.2 m Big refinement box: 0.4 m Small refinement areas: 0.1 m	14838549 cells

Table 4.1: Properties of each resolution of the mesh independence test

Figure 4.1 shows that the medium mesh values for all fields are closer to the fine mesh values. This means that a finer mesh will not significantly change the fields values. This is also verified by Table 4.2 that shows low values (less or equal to 5%) for all fields. Consequently, the medium mesh passes the mesh independence check, the first mesh verification check.

4.1.2 Residuals

For the basic case, it was setup with 5000 iterations to check the residuals. Figure 4.2 shows that all fields converge. Also, the relative difference between the runs is lower than the threshold.

However, creating a mesh where all fields' residuals converge for a thousand samples with different geometries is not an evident task. If perfect convergence cannot be achieved, at least the residuals should be low enough and the difference at the probes is lower than the threshold. After running the SA with

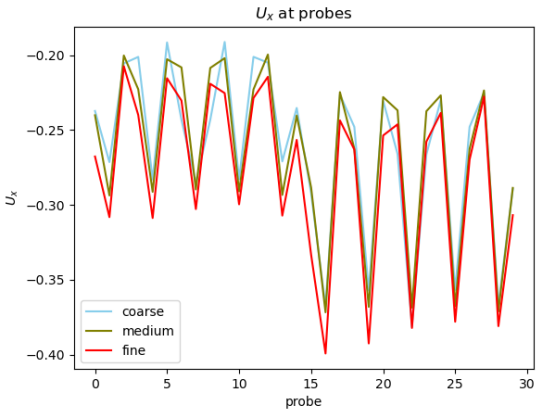

(a) U_x plot for all three meshes

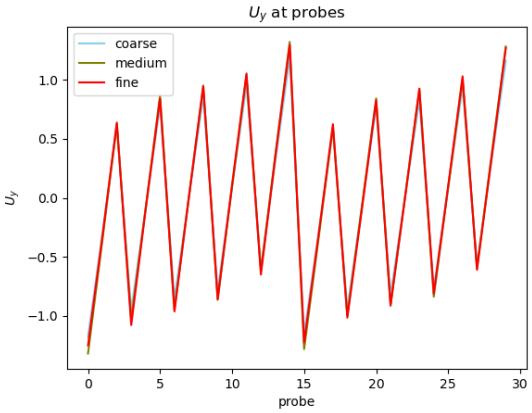

(b) U_y plot for all three meshes

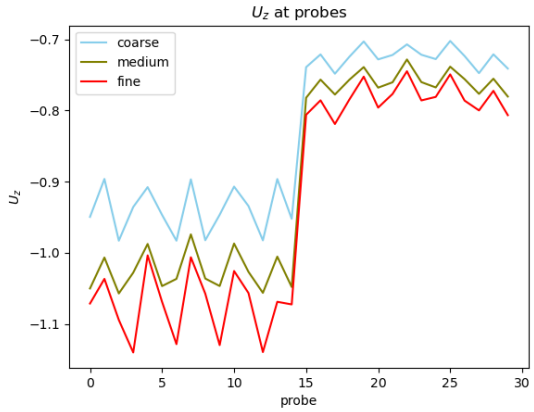

(c) U_z plot for all three meshes

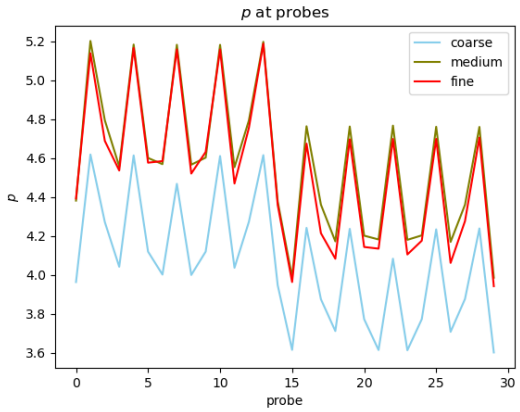

(d) p plot for all three meshes

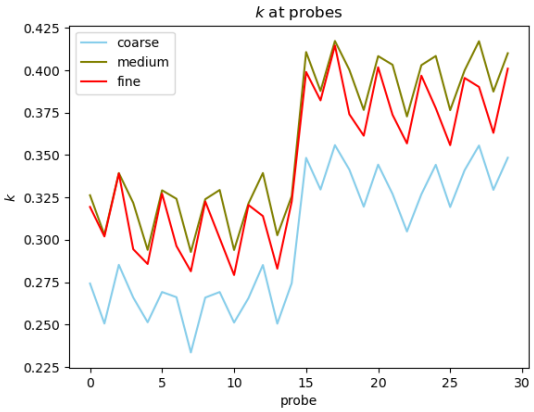

(e) k plot for all three meshes

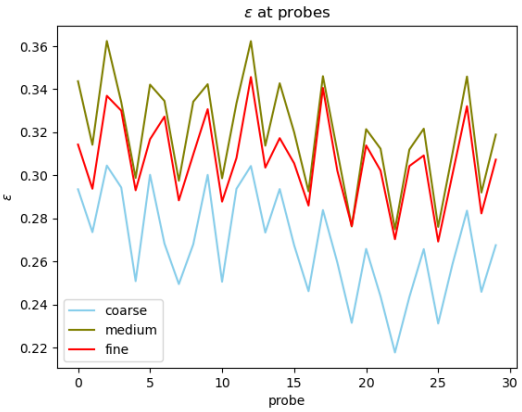

(f) ϵ plot for all three meshes

Figure 4.1: Mesh independence plots

Field	Median		
	e_a^{21}	e_{ext}^{21}	GCI_{ext}^{21}
U_x	5.3%	2.6%	3.4%
U_y	3.6%	2.3%	2.9%
U_z	3.1%	3.5%	4.5%
p	1.1%	0.1%	0.2%
k	3.5%	0.8%	1.0%
ϵ	3.4%	1.0%	1.3%

Table 4.2: Mesh independence results

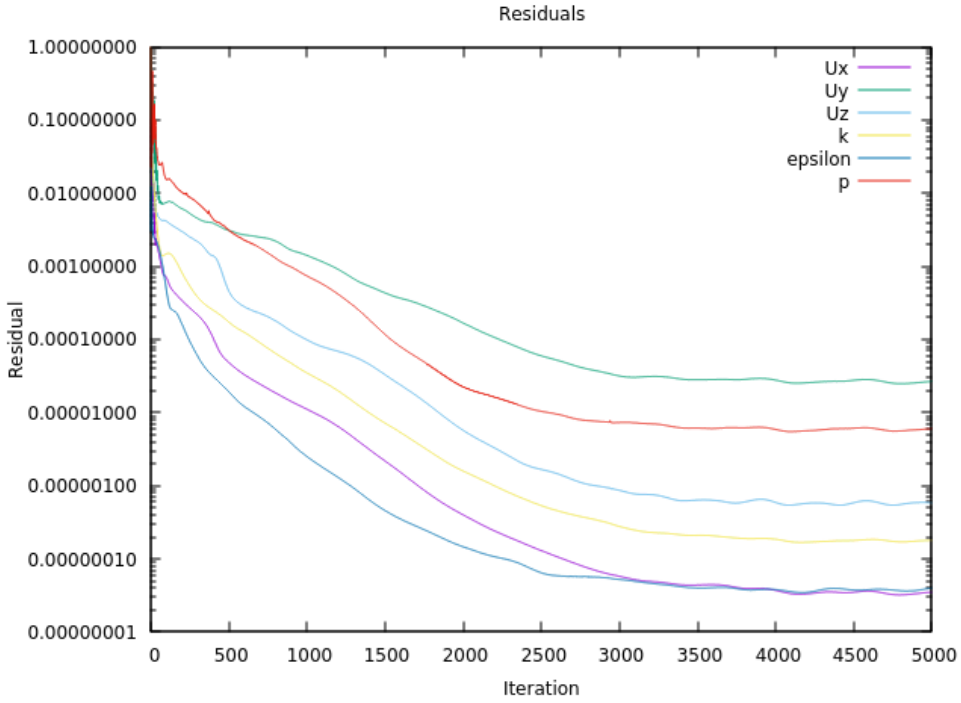

Figure 4.2: Residuals of fields of basic case

3000 iterations, a few samples were checked for convergence. It seems that some samples do converge (see Figure 4.3a) while others might still need a few extra iterations (see Figure 4.3b). Nevertheless, residuals are small enough, especially for the velocity components, to consider that this mesh passes the residuals check, the second mesh verification check.

4.2 Sensitivity Analysis

4.2.1 ANOVA results

Figure 4.4 shows that both α and β have p-values lower than the 0.05 threshold that indicates a 95% confidence interval for the sensitivity.

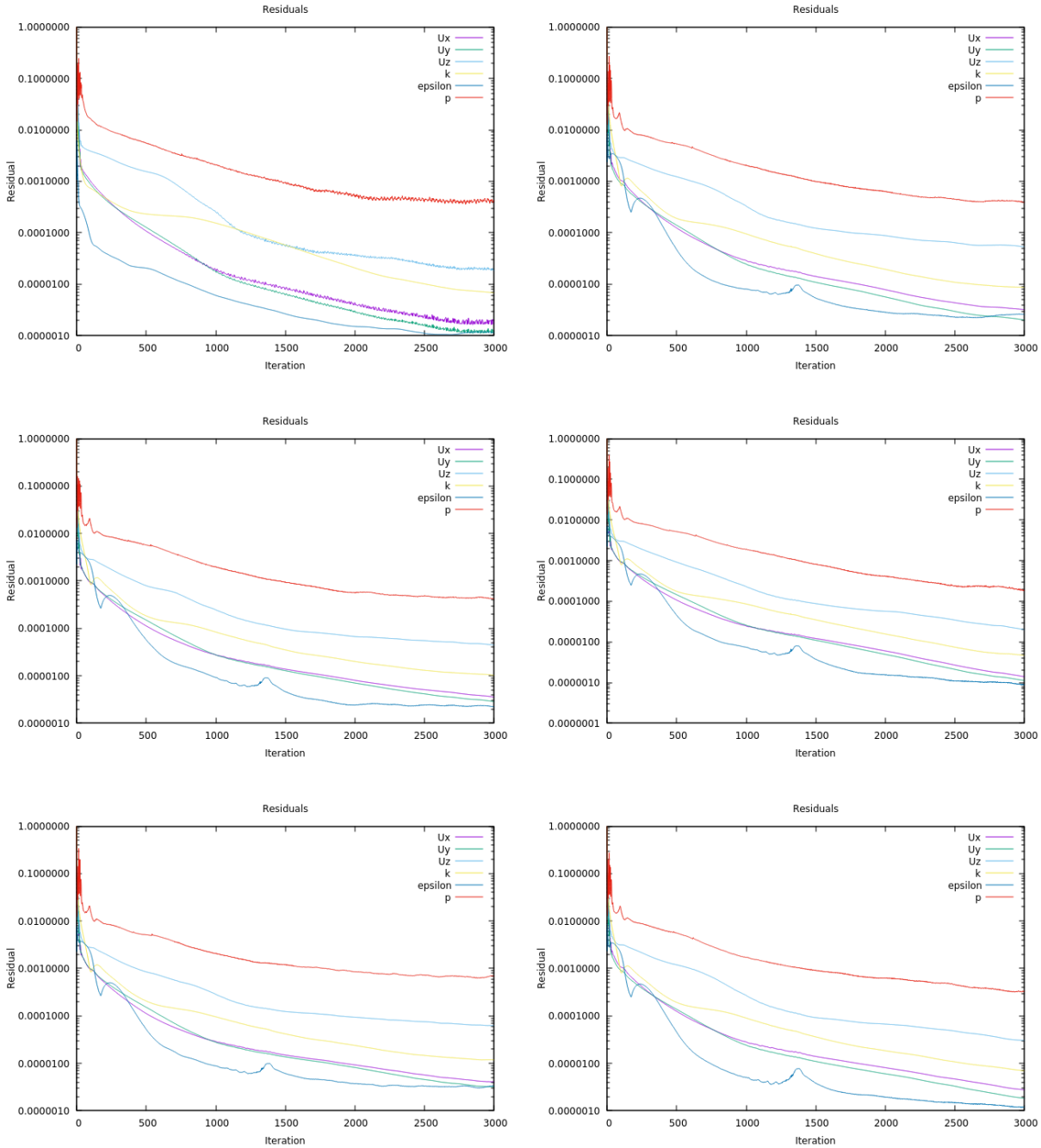

(a) Three residual plots where fields converge

(b) Three residual plots where fields do not converge

Figure 4.3: Different residuals of different samples

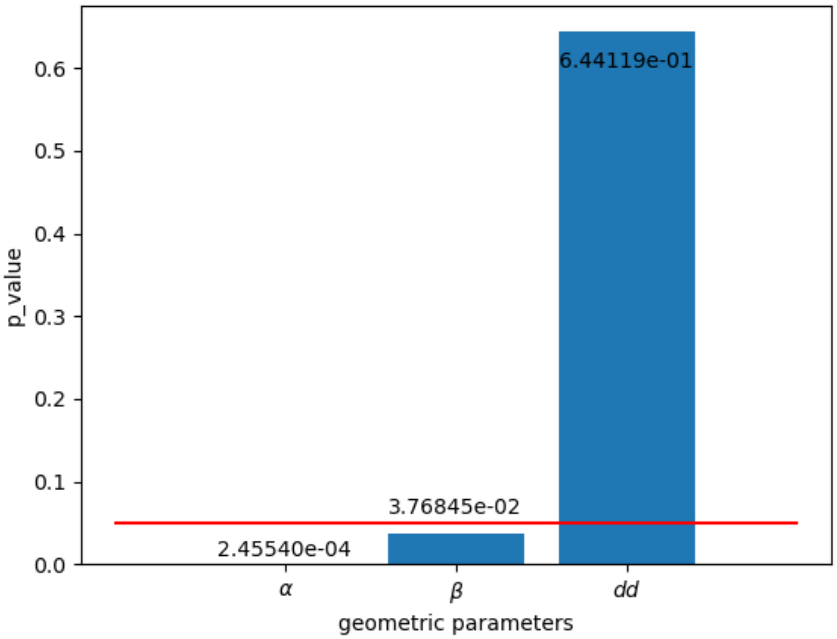

Figure 4.4: Bar plot showing the respective p-values of the geometry parameters from the ANOVA. The red line is the 0.05 limit for the 95% confidence interval

4.2.2 Discussion of results - chosen parameters

The difference in sensitivity between α and β shows that, given one wind direction, rotating the houses individually has more impact on widening the dunes than rotating the entire configuration. This means that, with an inter-distance of one-time the width of the houses, the acceleration that occurs between the houses is not negligible.

Therefore, the chosen parameters for optimisation are α and β. To fix dd, a linear regression was deduced from the samples obtained from the SA. Since the aim to widen the dunes involves minimising q, the difference of transport rate of Equation 3.14, the choice of dd should be the linear regression's value that gives the minimum q detected (see Figure 4.5).

Consequently, the minimum q is reached at dd = 4.66 m. This value is rounded to the closest integer because, on site, such a precision is difficult to obtain especially that dunes are not straight lines in real life. This means that, for the optimisation algorithm, dd is set to 5 m.

4.2.2.1 Comparison to previous studies

In Hoonhout and van Thiel de Vries [2014], a study conducted at Deltares about promoting the formation of dunes, it was recommended to use a 5 m distance to the dunes. However, van Onselen [2018] argues that a larger distance, up to 10 m, should be set to give more room for the formation of dunes. van Onselen [2018]'s study has a similar approach as this study; however, the parameters tested are inter-distance between the houses, houses elevated on poles and distance to dunes. Concerning the distance to dunes, both this study and van Onselen [2018]'s study conclude on the low influence this parameter has on the formation of dunes. For this reason, the distance to dunes could be set to 5m to benefit from the most wind deceleration if beach houses are removed during winter seasons. This way, during each installation, houses are moved as much as the dunes have grown. It could also be increased to 10 m in case the beach houses are permanent structures leaving more room for the dunes to grow.

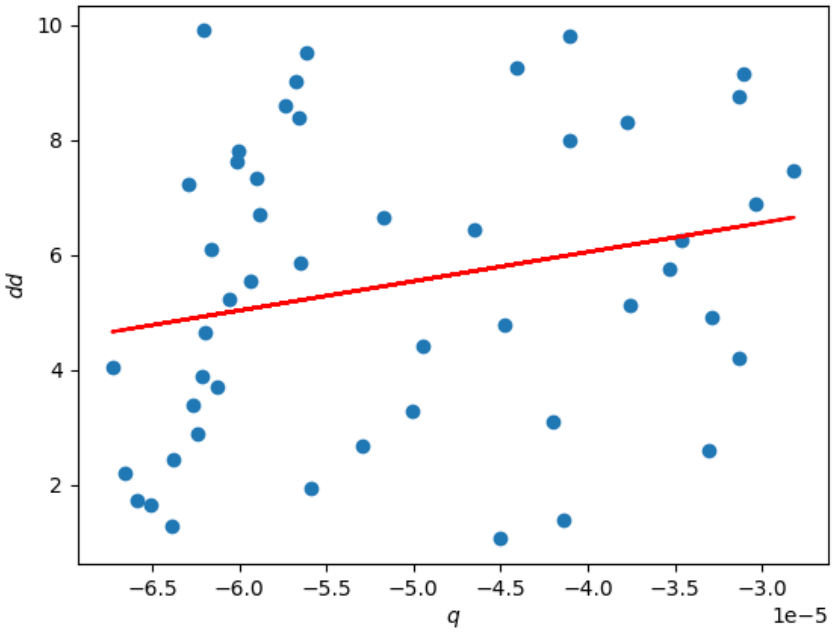

Figure 4.5: Linear regression (red line) for *dd* based on the sensitivity analysis samples (blue dots)

4.3 SBO

4.3.1 SBO results

4.3.1.1 Optimum prediction from surrogate

After getting the surrogate, several interpolation methods were conducted to try to predict an optimum (see Figure 4.6). The linear interpolation is the interpolation method that honours the data points the most; however, it does not allow for extrapolation to cover the whole interpolated domain. This means that a linear interpolation might miss a minimum outside of the concave hull defined by the samples. The minimum yielded from the linear interpolation (see Figure 4.6a) is a configuration with $\alpha = 31°$ and $\beta = 1°$.

The RBF interpolation allows extrapolation because it depends on the distance between a center point and the interpolated point. However, when Figure 4.6b is compared to Figure 4.6a, it seems that the trend shifts slightly when interpolated with RBF, especially at higher values of α and β. The minimum yielded from the RBF interpolation (see Figure 4.6b) is a configuration with $\alpha = 0°$ and $\beta = 0°$.

Kriging also allows extrapolation because it creates a statistical model from the surrogate's samples. Figures 4.6a and 4.6c show a very similar trend. This explains why kriging is usually favored to the other interpolation schemes because the statistical model can extrapolate values and respects the sample points. The minimum yielded from the kriging (see Figure 4.6c) is a configuration with $\alpha = 0°$ and $\beta = 0°$, which is the same minimum given with RBF.

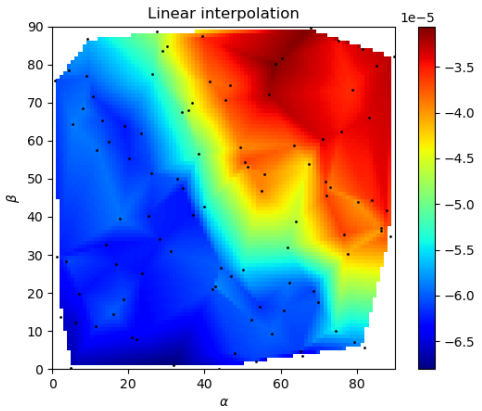

(a) Linear interpolation of the surrogate model

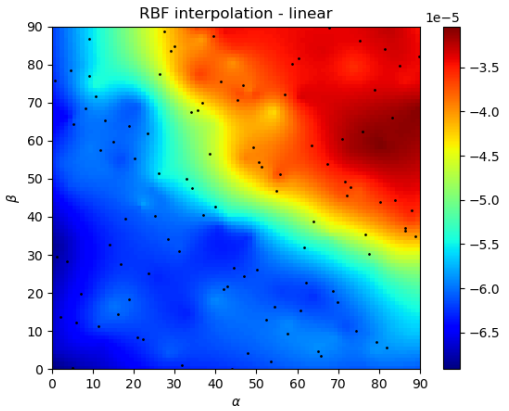

(b) RBF interpolation of the surrogate model

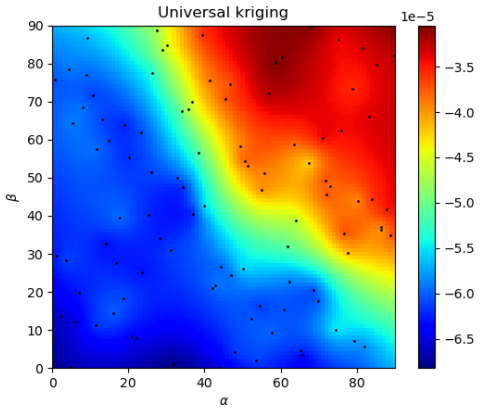

(c) Kriging interpolation of the surrogate model

Figure 4.6: Different interpolation schemes to try to predict the optimum. The dots in the graph represent the samples used to generate the surrogate, the color bar represents the values of q

4.3.1.2 Prediction from surrogate and first generation

After generating the first generation of the GA, the average relative error between the "truth" values and the interpolated values was computed using the following equation:

$$e = \left| \frac{truth - interpolated}{truth} \right| \times 100 \tag{4.1}$$

The average relative error of the surrogate is around 6%. This error value means that the surrogate is reliable to deduce a trend but not to deduce the optimum. For this reason, the first generation GA is added to the surrogate samples and interpolation is repeated (see Figure 4.7).

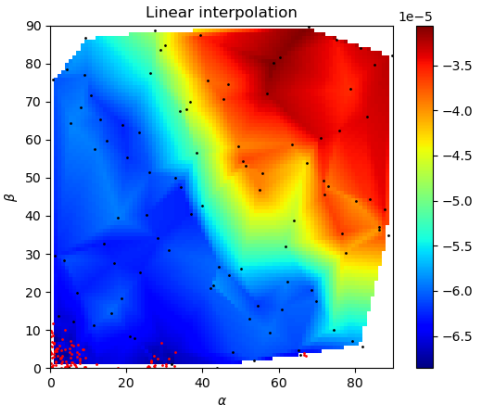

(a) Linear interpolation of the surrogate model with the first generation of the GA

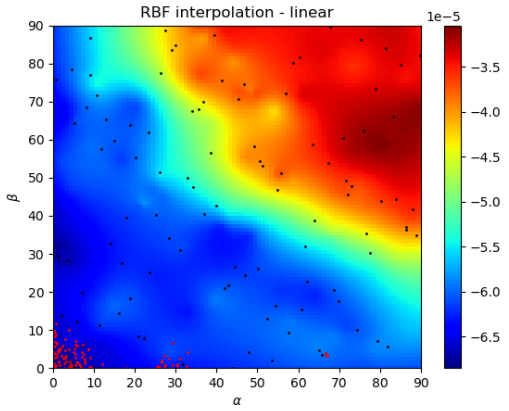

(b) RBF interpolation of the surrogate model with the first generation of the GA

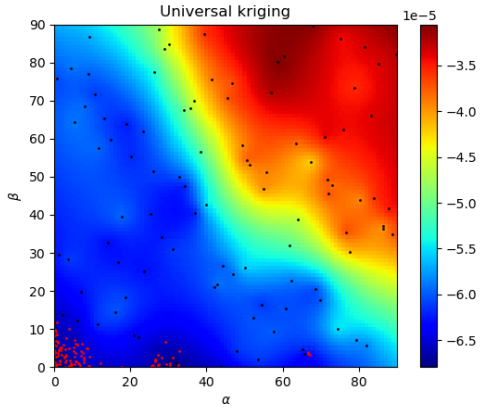

(c) Kriging interpolation of the surrogate model with the first generation of the GA

Figure 4.7: Different interpolation schemes with the first generation of the GA to try to predict the optimum more accurately. The black dots in the graph represent the samples used to generate the surrogate, the red dots represent the first generation GA, the color bar represents the values of q

First, the first generation seems to have located three minima regions and is converging towards one global minimum. Second, all three interpolations give the same interpolated minimum which is the configuration with $\alpha = 1°$ and $\beta = 4°$. This indicates that the model is becoming more accurate and this configuration will most likely be the optimum solution.

4.3.1.3 Trends detected

The trend is based on the kriging interpolation with first generation of the GA (see Figure 4.7c); however, any other interpolation graph yields approximately similar trends.

α In general, for a given β value, the larger α is, the larger the transport rate difference q is. However, this does not necessarily apply in the blue triangle area in Figure 4.7c. There are local maxima and minima along one value of β.

β seems to be generally varying in the same trend as α. In general, for a given α value, the larger β is, the larger q is. However, this also does not apply in the blue triangle area in Figure 4.7c. There are local maxima and minima along one value of α.

It should also be noted that, for a high value of α, a low β value lowers q. For a high value of β, a low α value lowers q. q is at its lowest when both α and β are low, and especially when β is low because of the three local minima regions detected by the GA.

4.3.1.4 Wind-facing surface

To try to link the local bumps seen in the interpolated graphs with the wind-facing surface, it was decided to get the total wind-facing surface of the configurations A, the wind-facing gap areas substracted from the total wind-facing surface of the configurations A_S and the ratio r of A_s over A. Linear regression is used to predict the general trend between the wind-facing surface and the output q.

Figure 4.8a shows that q increases when A_S increases resulting in an upward trend. This was not expected and needed further investigation resulting in plotting q with r and later fixing α and β to better analyse how the wind-facing surface affects q. Figure 4.8b shows a downward trend meaning that with no gaps in the wind-facing surface, it is more likely to have more sedimentation. Figure 4.8c only plots samples with no gaps in the wind-facing surface and constrains β to a low value. As expected, it shows a downward trend when the wind-facing surface is larger. Figure 4.8d filters the samples plotted in Figure 4.8c by constraining α to a low value. As expected, it shows a downward trend when the wind-facing surface is larger.

4.3.1.5 Accounting for different wind directions

To incorporate the effect of different wind directions into this study, twelve directions for the predicted optimum configuration were run (see Figure 4.9). Their results are weighted and added to conclude on the relative difference that would occur between the result from one dominant wind direction and the result of all twelve directions. There is a 6.8% increase between the q for the 60° wind direction and q from all weighted twelve wind directions (see Table 4.3).

4.3.2 Discussion

4.3.2.1 α

When α is low, the houses are not parallel to the dominant wind direction which means that the gaps between the houses are not completely facing the wind. Thus, the configuration acts as one block in the face of the wind (see Figure 4.10a). The larger α becomes, the more the houses are oriented towards the dominant wind direction, allowing for less deceleration to reach L2 (see Figure 4.10b and 4.10d). This was not expected when α is larger than 70° because, theoretically, the inter-distance flips to the shorter side of the houses making the larger side of the houses facing the dominant wind direction and increasing the wind-facing surface. However, further investigation shows that, in these cases, gaps are

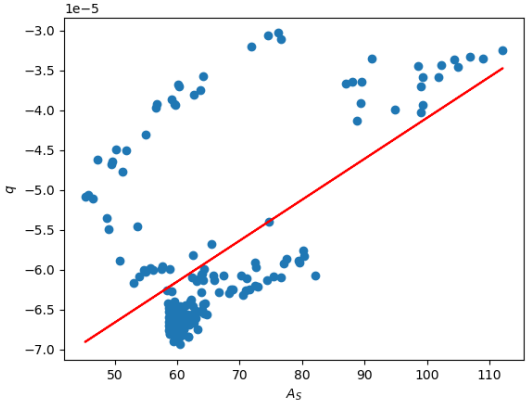

(a) Scatter plot showing the change in q when the A_S changes

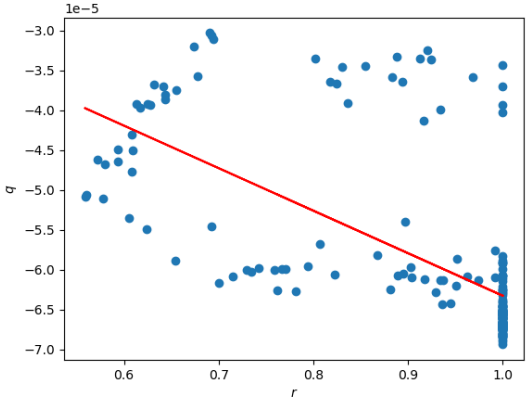

(b) Scatter plot showing the change in q when the r changes

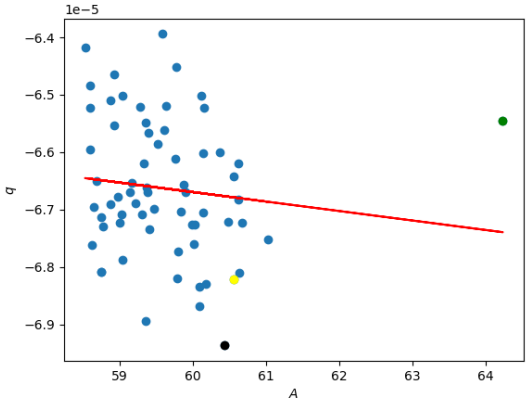

(c) Scatter plot showing the change in q when A changes, only accounting for the samples with $r = 1$ and $\beta < 4$

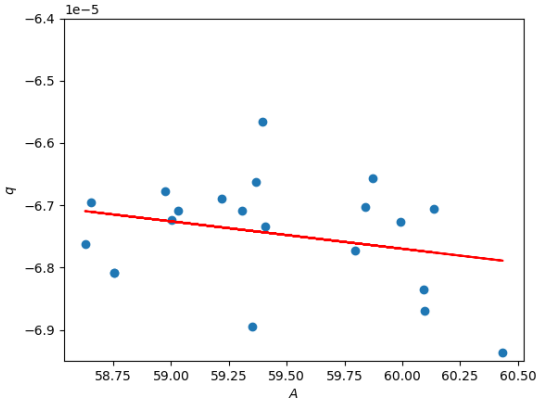

(d) Scatter plot showing the change in q when the A changes, only accounting for the samples with $r = 1$, $\beta < 3.8$, $\alpha < 3.8$

Figure 4.8: Wind-facing area analysis. The red line shows the linear regression line of each scatter plot

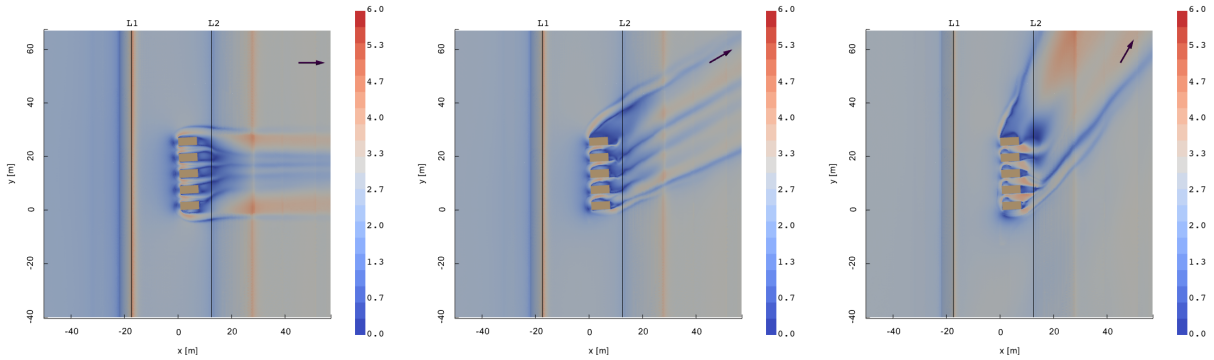

(a) Velocity field for $w = 0°$ (b) Velocity field for $w = 30°$ (c) Velocity field for $w = 60°$

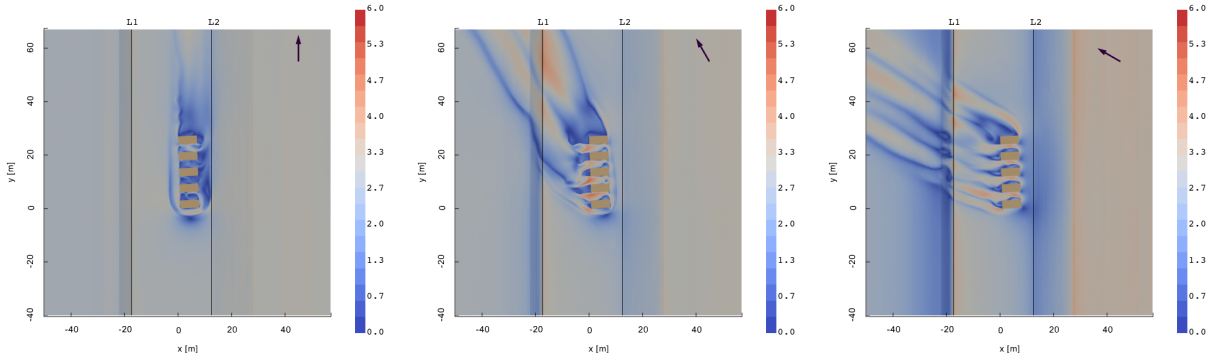

(d) Velocity field for $w = 90°$ (e) Velocity field for $w = 120°$ (f) Velocity field for $w = 150°$

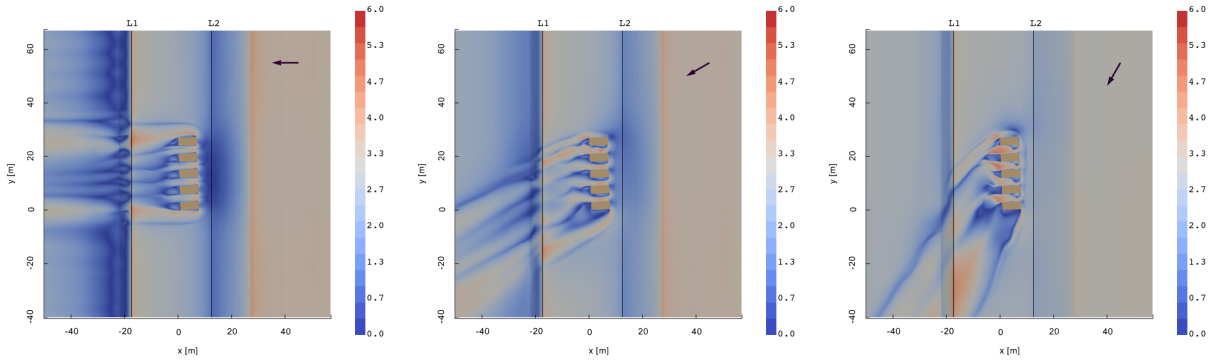

(g) Velocity field for $w = 180°$ (h) Velocity field for $w = 210°$ (i) Velocity field for $w = 240°$

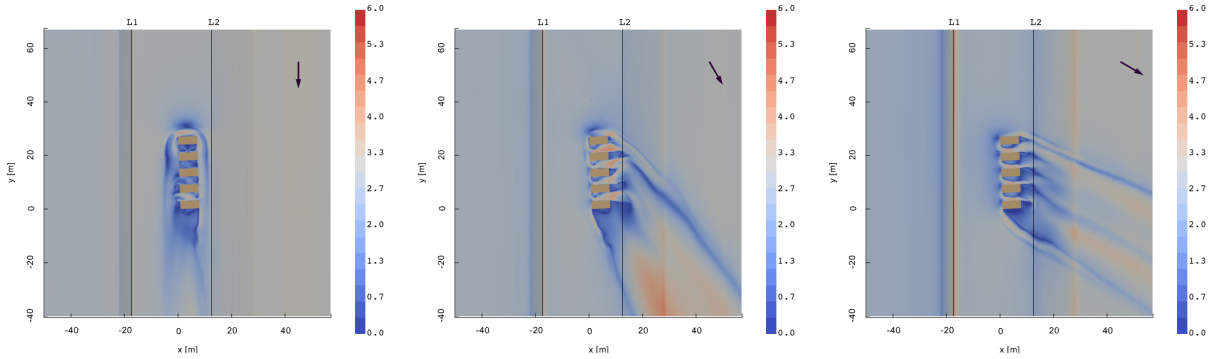

(j) Velocity field for $w = 270°$ (k) Velocity field for $w = 300°$ (l) Velocity field for $w = 330°$

Figure 4.9: The twelve directions run with the predicted optimum. L1 and L2 represent the samples lines and the arrow indicated the wind direction

w	q	Weight	Total
0	-0.00143	0.05	$-7.2*10^{-5}$
30	-0.00097	0.2	$-1.95*10^{-4}$
60	-0.00031	0.3	$-9.3*10^{-5}$
90	0	0.05	0
120	0.000305	0.15	$4.6*10^{-5}$
150	0.000774	0.025	$1.9*10^{-5}$
180	0.000904	0.025	$2.3*10^{-5}$
210	0.000759	0.05	$3.8*10^{-5}$
240	0.000292	0.03	$0.9*10^{-5}$
270	0	0.02	0
300	-0.00031	0.05	$-1.6*10^{-5}$
330	-0.00096	0.05	$-4.8*10^{-5}$
Total		1	$-2.89*10^{-4}$

Table 4.3: Results of each direction with its weight

limited with a shorter distance not allowing enough overlap between the houses and consequently not enough deceleration reach L2 (see Figure 4.10c).

4.3.2.2 β

When β is low, the configuration maintains a consistent distance to the dunes. The wake behind the houses that holds the most deceleration reaches the dunes over the whole configuration. However, when β is larger, the configuration as a whole starts taking a considerable distance from L2 (see Figure 4.11). If one point of the configuration is at 5 m from the dune, other points are at 20 m away from the dunes. This leaves room for the flow to start reattaching again and accelerating when it gets to the dune's foot. Figure 4.11a and 4.11b show that a lower α helps increase the overlap between the houses and significantly reduce velocity in the wake region even though both configurations present gaps when facing the wind dominant direction.

4.3.2.3 Combining α and β

The combination of α and β can affect the gaps size, the overlap between the houses, and the wind-facing surface. This can explain why the interpolation graphs show certain local maxima in regions where a lower value is expected. Figure 4.12 shows three samples that can be mapped to the interpolation in Figure 4.7c as follows: Figure 4.12a shows a sample with a 1% higher q than samples depicted in Figure 4.12b and 4.12c, even though the former sample has a lower combination of α and β. This is mainly a combination of how aligned the houses are with the dominant wind direction and how aligned the gaps are with the with the dominant wind direction when combining α and β.

4.3.2.4 Wind-facing surface

Figure 4.8a shows that q is higher with a higher A_S. This is misleading because subtracting the gaps from A does not account for the effect of those gaps, i.e.the effect of α, nor does it account for the effect of β. However, when Figure 4.8b takes the ratio of A_S over A, it considers the effect of the gaps. This gives a downward trend as expected. The more the configuration works as one block, the more sedimentation there is. The reason that not all samples with a ratio of 1 have a lower q is mainly attributed to having a larger β. To try to restrain β, the same plot in Figure 4.8b is repeated with only $\beta < 4$ in Figure 4.8c.

Figure 4.8c shows a downward trend; however, there are a few cases where a wider area might not necessarily result in a lower q. There are two reasons for that; each category is marked with a different

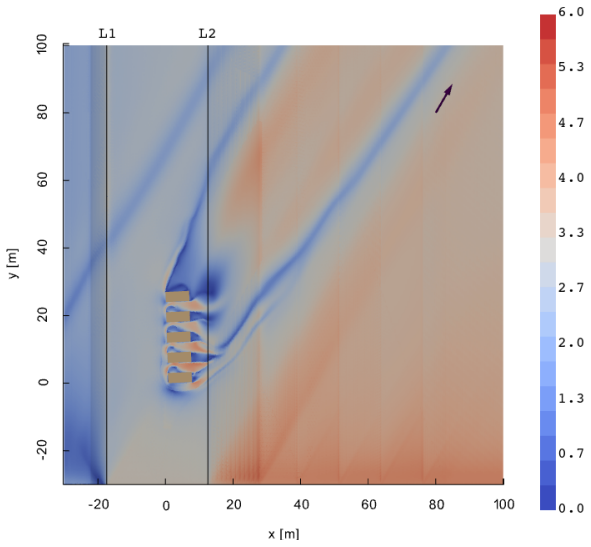

(a) Sample with $\alpha \approx 1°$ and $\beta \approx 3.8°$ - best-performing configuration

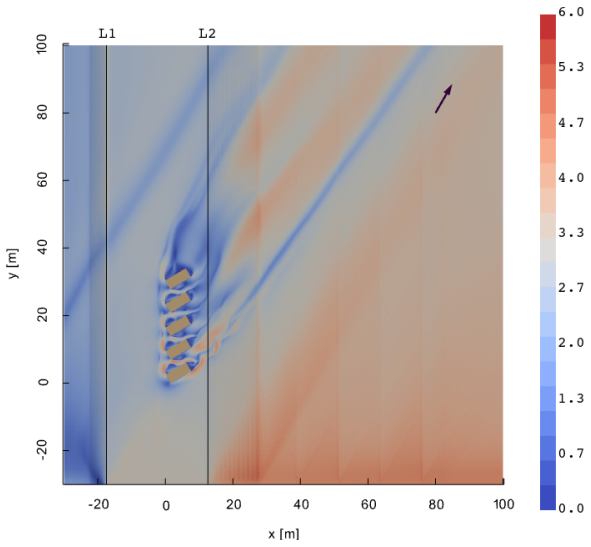

(b) Sample with $\alpha \approx 30°$ and $\beta \approx 0.5°$

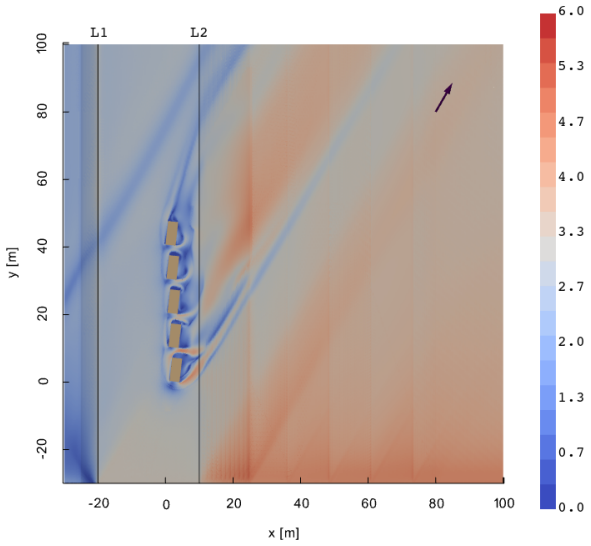

(c) Sample with $\alpha \approx 82°$ and $\beta \approx 6°$

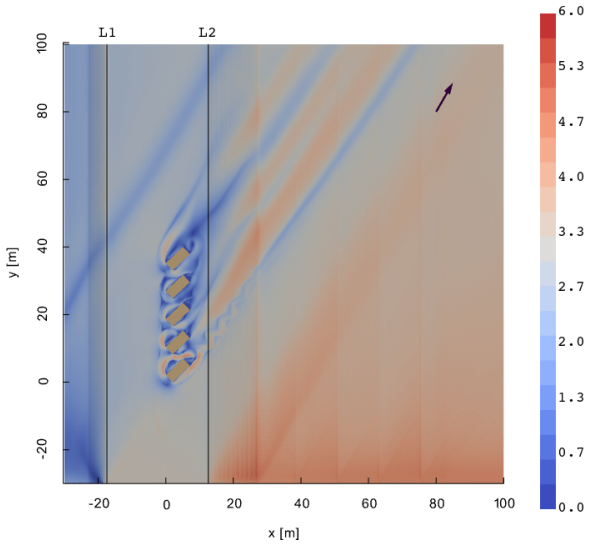

(d) Sample with $\alpha \approx 44°$ and $\beta \approx 0°$

Figure 4.10: Configurations showing how α affects the velocity field when β is low

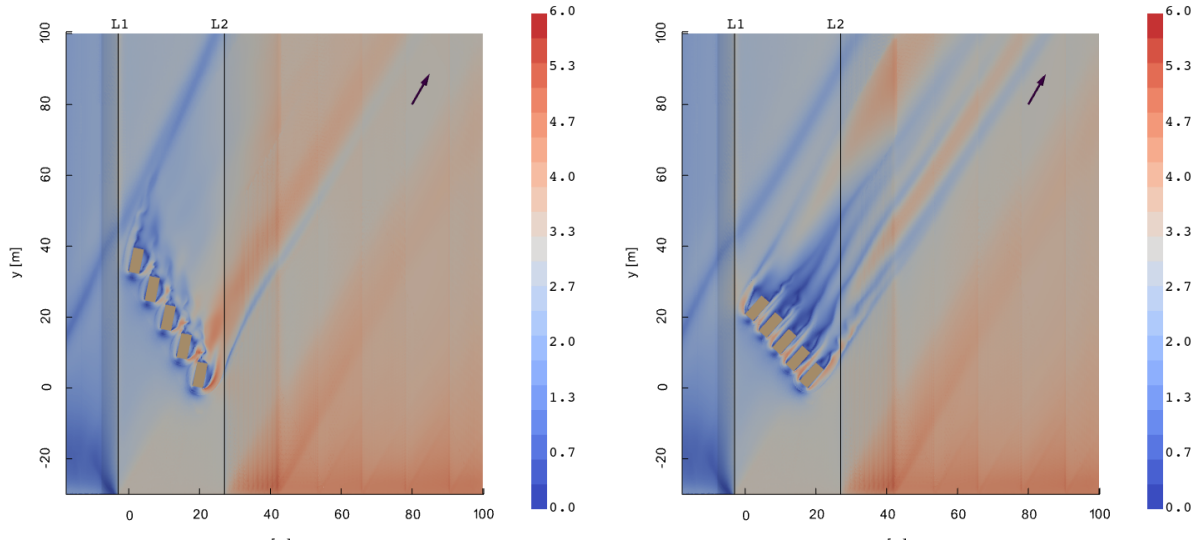

(a) Sample with $\alpha \approx 59°$ and $\beta \approx 80°$ - worse-performing configuration

(b) Sample with $\alpha \approx 9°$ and $\beta \approx 87°$

Figure 4.11: Configurations showing how α affects the velocity field when β is high

color in Figure 4.8c. The first reason for the change is a different β. For instance, The yellow dot sample has a slightly wider β than the black dot sample causing the 1% increase in q. The second reason for the change is, that even though the configuration does form one block from the wind direction, the amount of overlap between the houses is also important. In the case of the green dot sample (see Figure 4.10d), the overlap is far less than in the case of the black dot sample (see Figure 4.10a). When both α and β are restricted to small values, the smallest q is indeed for the largest wind-facing area (see Figure 4.8d. This explains why a configuration with $\alpha = 1°$ and $\beta = 4°$ performs better than a configuration with $\alpha = 0°$ and $\beta = 0°$. The former configuration gives larger wind-facing surface resulting in a 2% increase of sedimentation. Figure 4.8 shows that increasing the wind facing surface in absolute value does not immediately mean more sedimentation. Instead, α and β need to be carefully designed before maximising the wind-facing surface. This highlights the complexity of the system when α and β change and their impact on other dependent variables such as the overlap between the houses and the wind-facing surface.

In conclusion, the criteria for an optimal design that promotes widening of dunes are:

1. α should be defined in a way that the houses are not parallel to the dominant wind direction, reducing wind-facing gaps;
2. α should also allow for enough overlap between the houses;
3. β should keep the configuration as consistently close to the dunes foot as possible
4. When all three above criteria are respected, the wind-facing surface should be maximised.

It should be noted that good-performing configurations can be obtained by only respecting three out of the four previous criteria, as long as they fall in the blue triangle area of Figure 4.7c.

4.3.3 Updating predicted optimum

After running 400 samples (the surrogate and three generations), the interpolated optimum is the configuration with $\alpha = 1°$ and $\beta = 3°$. The interpolated optimum is shifting less, and this indicates that the surrogate is becoming more and more accurate, validating the earlier chosen optimum.

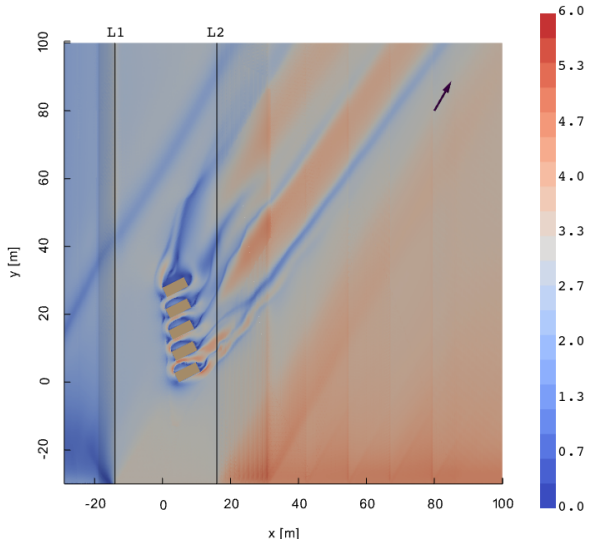

(a) Sample with $\alpha \approx 19°$ and $\beta \approx 18°$

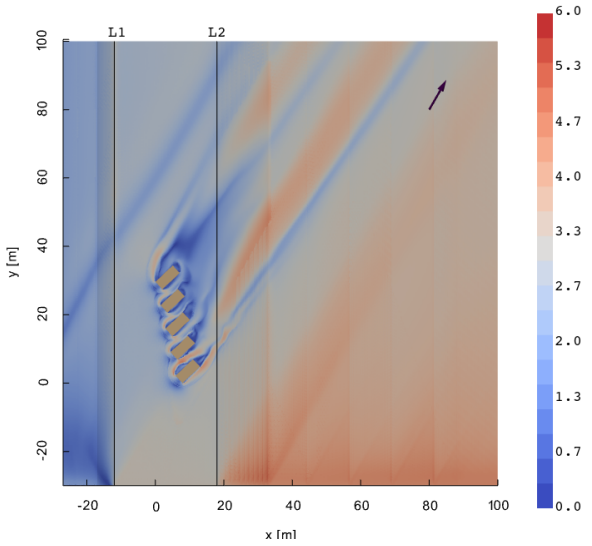

(b) Sample with $\alpha \approx 31°$ and $\beta \approx 30°$

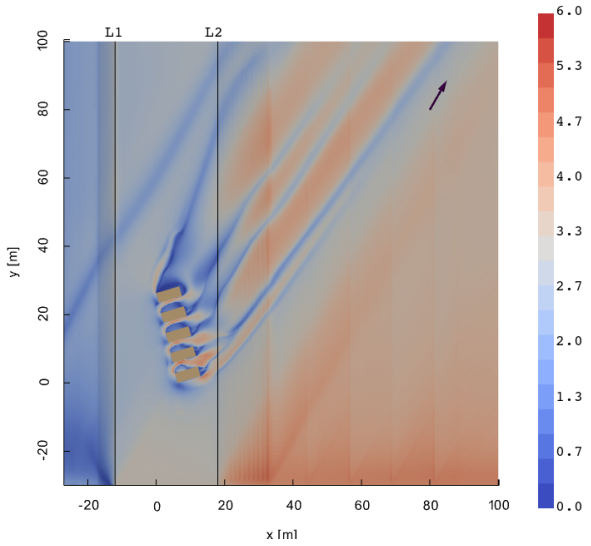

(c) Sample with $\alpha \approx 4°$ and $\beta \approx 28°$

Figure 4.12: Configurations showing how α and β affect the velocity field when they change together

5 Conclusion

The natural nourishment of dunes is a resilient approach to maintain an important defence system in the face of rising coastal hazards. Based on the idea of PBD, the aim of this project is to investigate geometric design parameters to promote the formation of dunes by widening them. The study has combined parametric design and automated CFD simulations approach to analyse the sensitivity of the configuration towards variable parameters, deduce the trends that are defined when the parameters change and optimise the combination of influential geometric parameters to increase sedimentation. For the parametric design, three geometric variables were studied:

- α: rotation angle of individual houses relative to shoreline
- β: rotation angle of configuration relative to the shoreline
- dd: distance of configuration to the foot of the dunes

The novelty of this work, compared to available studies, is the introduction of those two angles, α and β.

To identify the most influential parameters, a sensitivity analysis was performed. It was found that α and β are the most influential parameters of the three geometric variables. Despite its relative lower influence, dd was chosen to best lower the velocity behind the configurations.

After setting dd, a surrogate model was built from α and β to predict an optimum and run a SBO. The predicted optimum was derived three times as follows:

- Surrogate model (100 samples): optimum configuration has $\alpha = 0°$ and $\beta = 0°$;
- Surrogate model and first generation GA (200 samples): optimum configuration has $\alpha = 1°$ and $\beta = 4°$;
- Surrogate model and three generations GA (400 samples): optimum configuration has $\alpha = 1°$ and $\beta = 3°$;

With 400 samples, the best configuration concluded has the following properties:

- $\alpha = 1°$;
- $\beta = 3°$;
- $dd = 5$ m;

However, it is not only a matter of just one optimum; several trends were found to create design guidelines for optimal beach houses configurations. For this reason, four design criteria can be concluded to help increase sedimentation:

1. α should be defined in a way that the houses are not parallel to the dominant wind direction, reducing wind-facing gaps;
2. α should also allow for enough overlap between the houses;
3. β should keep the configuration as consistently close to the dunes foot as possible
4. When all three above criteria are respected, the wind-facing surface should be maximised.

Finally, the conclusions about the gaps, the overlap and the wind-facing surface can be used when considering new parameters or parameters that were constants in this study. For instance, wider or larger beach houses might result in more sedimentation because it increases both the overlap and the wind-facing surface. Increasing the number of houses used in a configuration could also help with increasing the wind-facing surface. This could also be extended to working with row configurations. Placing rows in a way that gaps are closed and wind-facing surface is maximised can have an impact on increasing sedimentation on the foot of the dunes. This could help configurations that performed poorly in this study to perform significantly better when correctly stacked in rows of houses.

5.1 Answers to research questions

Wind simulation

- What is a suitable computational domain and mesh for the scenarios to be tested?
  The dimension of the domain should follow the guidelines presented in Blocken [2015] resulting in this case with a 205*330*81 m domain. As for the mesh, the areas of interest near the houses and in the wake area should have the smallest refinement cells. The terrain surface should also be refined to ensure mesh independence and better convergence of residuals. Then, an intermediate refinement box separates the interest area with small refinement cells from the coarse background cells. See section 3.4.3 for more detail.

Housing configurations

- What are the parameters to define these house configurations?
  There are several parameters that define the beach house configurations. Some parameters are constant in this study and others are variables and will be investigated throughout the work. The constant parameters are length of a house L, width of a house l, height of a house h, and inter-distance between houses d. The variable parameters are rotation relative to the shoreline of individual houses α, rotation relative to the shoreline of the entire configuration β, distance of configuration to dunes dd.

- Which parameters are more influential on the formation of the dunes?
  Based on a sensitivity analysis run with the three variable parameters, the most influential parameters are α and β.

Formation of dunes

- How to factor in the wind direction in the final configuration choice?
  In this study, all simulations were run using one dominant wind direction 60°, and the optimal configuration was run with twelve weighted wind directions depending on their yearly occurrence. This allowed to quantify the relative difference that occurs when factoring in all different wind directions and when factoring in only the dominant wind directions.

- How to evaluate the widening of the dunes?
  A line method has been implemented. It takes the beginning of the plateau, line 1 (L1) and the end of the plateau, i.e. the foot of the dune, line 2 (L2) and gets the difference in transport rate between L2 and L1. To get the transport rate at each line, the velocity field is sampled on these lines at a 30 cm height. The larger the negative difference is, the more sedimentation stays on the plateau.

Main research question

- Based on wind simulation, which beach house configuration best promotes widening of dunes? As concluded earlier, the best configuration has the following properties:
  - $\alpha = 1°$;
  - $\beta = 3°$;
  - $dd = 5$ m;

5.2 Limitations

The main limitations of this study are the following:

1. The mesh in refinement boxes for some cases presents inconsistent cell sizes. This is mainly due to the black box settings of automatic meshers. However, consistent refinement always reaches the foot of the dunes, i.e. L2, where fields are sampled for output. This could slightly be more problematic if this mesh will be used for heightening of the dunes;

2. A few assumptions have been made in setting up the model, such as simplifying the cross-section of the Dutch coast, not accounting for moisture and humidity, and not accounting for vegetation on the dunes. This would be particularly useful for accurately quantifying the sedimentation at the foot of the dunes;

3. For the optimisation, it was not possible to create integer domain variables in DAKOTA. Having integer domain variables could have reduced the time for convergence for the optimisation.

5.3 Recommendations and further improvements

Geometry

1. The inter-distance changes from being measured between the two larger sides of the houses to the two shorter sides after $\alpha = 70°$. It is recommended to reduce this angle to 45°. It is expected to reduce the three local minima regions from the interpolation. It could be that the region around $\alpha \approx 67°$ and $\beta \approx 2°$ becomes the new global optimum because that configuration will allow a significant overlap and a maximised wind-facing surface;

2. Based on van Onselen [2018], a smaller inter-distance allows for less acceleration between the houses, increasing sedimentation behind the houses. It could be interesting to test with a smaller inter-distance value to see if it increases the sedimentation and test how it interacts with α and β;

3. Based on the results of this study, it was concluded that the overlap between the houses is also an important factor that affects widening the dunes. For this reason, it is recommended to test α with [-90, 0] interval since it flips the gaps away from the dominant wind direction and increases the overlap. It would also be interesting to try to change the overlap with a fixed α and β and see the impact this has on the velocity field and consequently on the transport rate between L1 and L2.

CFD

1. CFD simulations can run with different roughness length for different parts of the coastal section, accounting for sea, sand and vegetated dunes. This helps with getting more realistic results when compared to on-site measurements instead of only relying on the relative difference between different configurations;
2. To get more accurate results, after detecting a regional minimum area, simulations can be run with LES providing more insight into how these regions vary;
3. The numerical model and the results need to be validated with on-site measurements. The trends from the interpolation should be compared to field findings to see if the assumptions affect those trends or not;
4. To account for the twelve wind directions for more than just the optimum configuration, it is recommended to create a pre-processing step where LHS sampling is used to generate a small number of samples that will be run with twelve wind directions, and the output is the relative difference between the dominant wind direction and all twelve directions. A response surface can then be fitted into these samples and used as a reference to estimate the relative difference for simulations that will only run for the dominant wind direction.

Optimisation

1. A comparison between a SBO GA and a SBO ACO can be conducted to see if it helps a faster convergence and more accurate outcomes. This should also take into account the more straightforward way to implement a SBO GA compared to a SBO ACO.

A Reproducibility self-assessment

A.1 Marks for each of the criteria

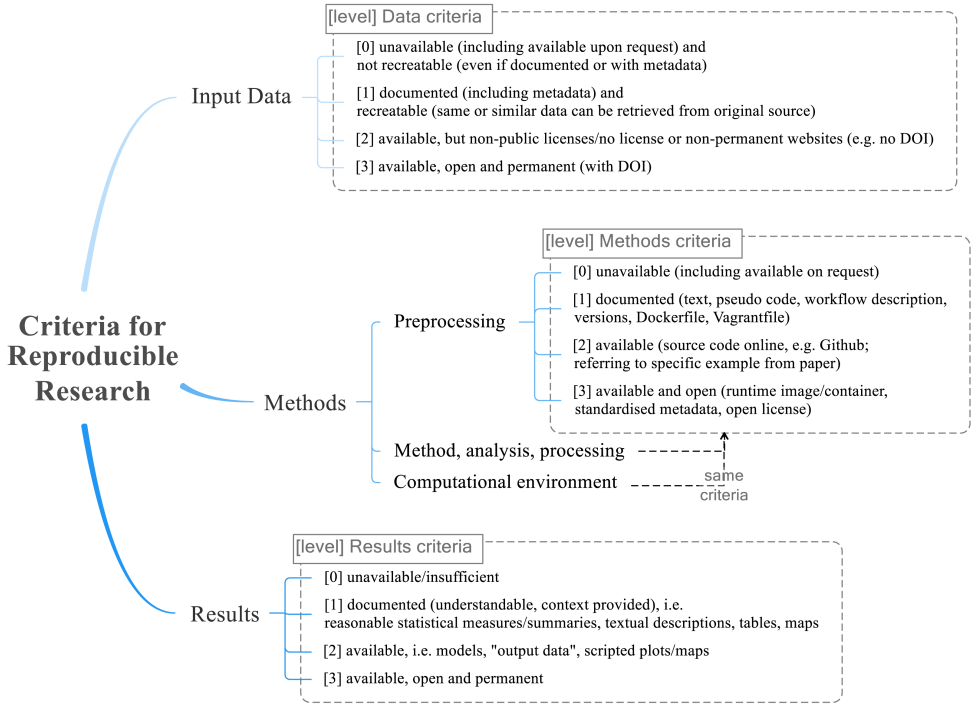

Figure A.1: Reproducibility criteria to be assessed. source: [Nüst et al., 2018]

Criteria	Grade	Justification
Input data	2	The profile and the houses are available on the Github page of the project but no DOI. They were modelled for the purpose of this study.
Preprocessing	3	Available and open on the Github page of the project but does not contain metadata yet.
Methods	3	Available and open on the Github page of the project but does not contain metadata yet.
Computational environment	3	Open source software
Results	1	The samples take up 1Tb of space and will not be hosted on Github; however, they are documented in the report and can easily be reproducible.

Table A.1: Reproducibility criteria grading for this study. (Project's Github page: `https://github.com/NadHobeika/dace_sensitivity_analysis`)

B Miscellaneous pseudo-code

This chapter gives the pseudo-code to generate the refinement lines and boxes for CfMesh and to get the wind facing surface and removing the gaps.

B.1 Generating refinement lines and boxes

For the terrain refinements, several lines need to be created to cover the whole rotated area of the refinements. These lines have an extent of 0.6 m, the height of refinement from the terrain. There are lines *hrzlines* for the plateau terrain refinements and other lines *slines* for the slopped terrain refinements. For the houses, each house requires one line to cover the whole box. The following pseudo-code applies for wind directions from 0° to ang90 not included. The code slightly changes for each quadrant.

Algorithm B.1: Generate refinement lines and boxes for CfMesh

Input: w, dd, houses file hh, x_total of houses bounding box $xbbox$
Output: lines and boxes text file f

$plateausample \leftarrow 0.3$;
$slopesample \leftarrow 2.8$;
$allpts \leftarrow$ extract all points from hh;
$obbcorners \leftarrow$ get oriented bounding box obb corners;
$obbcorners \leftarrow$ sort corners to always have same corners order;
$baseline \leftarrow$ offset wind-facing side of obb by 0.6;
$totaltodunes \leftarrow xbbox + dd$;
$baseline \leftarrow$ extend baseline to cover corners with angled wind directions;
$step \leftarrow 0.6$ / sin $anglebetweenwinddirectionandbaseline$;
$baseline \leftarrow$ extend baseline to have a full number of lines;
$linecount \leftarrow$ get number of lines to cover $baseline$;
$ptfootdunes \leftarrow$ get the intersection of the dunes foot with the wind vector originating from the first baseline point using $totaltodunes$;
$pttopdunes \leftarrow$ get the intersection of the dunes top with the wind vector originating from $ptfootdunes$;
$p0 \leftarrow$ first baseline point;
$p0 \leftarrow (p0[0], p0[1], plateausample)$;
$p1 \leftarrow (ptfootdunes[0], ptfootdunes[1], plateausample)$;
$p2 \leftarrow (pttopdunes[0], pttopdunes[1], slopesample)$;
for $i \leftarrow 0$ **to** $linecount$ **do**
    $f \leftarrow$ write $(p0 + (step * i))$ to file $f \leftarrow$ write $(p1 + (step * i))$ to file $f \leftarrow$ write $(p2 + (step * i))$ to file
$outerboxmax \leftarrow (p3[0] + 1, p3[1] + 1, 6)$;
$outerboxmin \leftarrow (p0[0] - 6, baseline[1][1] - 6, 0)$;
$centerouterbox \leftarrow (outerboxmax + outerboxmin) / 2$;
$totalouterbox \leftarrow (outerboxmax - outerboxmin)$;
$f \leftarrow$ write $outerboxmax$, $outerboxmin$, $centerouterbox$, and $totalouterbox$ to file;
$hh_i \leftarrow$ get houses points from hh;
for hh_{ii} *in* hh_i **do**
    $haxis \leftarrow$ get horizontal middle axis of house hh_{ii} $f \leftarrow$ write $haxis$ to file

B.2 Get full wind-facing surface

Instead of getting the projection on the plane perpendicular to the 60° wind direction, the houses were rotated 30° and thus only the x-axis is taken into account.

Algorithm B.2: Get full wind_facing surface

Input: houses file *hh*
Output: Wind_facing surface A

$hh_rotated \leftarrow$ rotate *hh* by 30°;
$allpts \leftarrow$ extract all points from *hh*;
$h \leftarrow$ 3 m;
$xmin \leftarrow$ get minimum x from $allpts$;
$xmax \leftarrow$ get maximum x from $allpts$;
$xtotal \leftarrow xmax\text{-}xmin$;
$A \leftarrow xtotal * h$;

B.3 Get wind-facing surface without the gaps

Algorithm B.3: Get wind-facing surface without the gaps

Input: houses file *hh*
Output: Wind_facing surface without gapsA_S

$hh_rotated \leftarrow$ rotate *hh* by 30°;
$allpts \leftarrow$ extract all points from *hh*;
$h \leftarrow$ 3 m;
$houses \leftarrow 5$;
$hh_0 \leftarrow$ extract all points of first house;
$hh_1 \leftarrow$ extract all points of second house;
$xmin_0 \leftarrow$ get minimum x from hh_0;
$xmax_0 \leftarrow$ get maximum x from hh_0;
$xmin_1 \leftarrow$ get minimum x from hh_1;
$xmax_1 \leftarrow$ get maximum x from hh_1;
if $xmin_0 \leq xmax_1$ **then**
    $xmin \leftarrow$ get minimum x from $allpts$;
    $xmax \leftarrow$ get maximum x from $allpts$;
    $xtotal \leftarrow xmax\text{-}xmin$;
    $A_S \leftarrow xtotal * h$;
else
    $xtotal \leftarrow xmax_0\text{-}xmin_0$;
    $A_S \leftarrow xtotal * houses * h$;

Bibliography

Adams, B., Ebeida, M., Eldred, M., Jakeman, J., Swiler, L., Stephens, J., Vigil, D., Wildley, T., Bohnhoff, W., Dalbey, K., Eddy, J., Hooper, R., Hu, K., Hough, P., Bauman, L., and Rushdi, A. (2014). DAKOTA , A Multilevel Parallel Object-Oriented Framework for Design Optimization , Parameter Estimation , Sensitivity Analysis , and Uncertainty Quantification Acknowledgment.

Amrouni, O. (2002). Stabilisation et réhabilitation des dunes bordières de la côte nord de mahdia (tunisie orientale).

Arens, S. M., Van Boxel, J. H., and Abuodha, J. O. (2002). Changes in grain size of sand in transport over a foredune. *Earth Surface Processes and Landforms*, 27(11):1163–1175.

Bagnold, R. (1941). The physics of blown sand and desert dunes. london: Methuen.

Bataleblu, A. (2019). Computational intelligence and its applications in uncertainty-based design optimization.

Blocken, B. (2015). Computational Fluid Dynamics for urban physics: Importance, scales, possibilities, limitations and ten tips and tricks towards accurate and reliable simulations. *Building and Environment*, 91:219–245.

Blocken, B. (2018). *LES over RANS in building simulation for outdoor and indoor applications: A foregone conclusion?*, volume 11.

Blocken, B., Stathopoulos, T., Carmeliet, J., and Hensen, J. L. (2011). Application of computational fluid dynamics in building performance simulation for the outdoor environment: An overview. *Journal of Building Performance Simulation*, 4(2):157–184.

Casella, S. G. (2020). Surrogate based optimisation for hull shapes with dakota toolkit. Master's thesis, Delft University of Technology.

Cavaglieri, D. (2016). New numerical methods for computational fluid dynamics, forecast and control.

Celik, I., Ghia, U., Roache, P., Freitas, C., Coloman, H., and Raad, P. (2008). Procedure of estimation and reporting of uncertainty due to discretization in cfd applications. *J. Fluids Eng.*, 130:078001.

CFDOnline (2010). Rng k-epsilon model. *CFD Online*.

Change, N. (2021). Arctic sea ice minimum — nasa global climate change.

Chaouat, B. (2017). The State of the Art of Hybrid RANS/LES Modeling for the Simulation of Turbulent Flows. *Flow, Turbulence and Combustion*, 99(2):279–327.

Chen, L.-T. and Peng, C.-Y. J. (2013). Constructing confidence intervals for effect sizes in anova designs. *Journal of Modern Applied Statistical Methods*, 12(2):82–104.

DeJong, K. A. (1975). *Analysis of the Behavior of a Class of Genetic Adaptive Systems*. Doctoral dissertation, The University of Michigan, Department of Computer and Communication Sciences Department.

Delgado-Fernandez, I. (2011). Meso-scale modeling of aeolian sediment input to coastal dunes. *Geomorphology*, 130:230–243.

Estrado, E. (2019). Optimisation of complex geometry buildings based on wind load analysis.

Forrester, A., Sobester, A., and Keane, A. (2008). Engineering Design via Surrogate Modelling: A Practical Guide. In *Engineering Design via Surrogate Modelling: A Practical Guide*.

García-Sánchez, C., Philips, D., and Gorlé, C. (2014). Quantifying inflow uncertainties for cfd simulations of the flow in downtown oklahoma city. *Building and Environment*, 78:118–129.

Georgiadis, N. J., Rizzetta, D. P., and Fureby, C. (2010). Large-eddy simulation: Current capabilities, recommended practices, and future research. *AIAA Journal*, 48(8):1772–1784.

Hachimi, H. (2013). Hybridations d'algorithmes métaheuristiques en optimisation globale et leurs applications.

Hesp, P. A. and Smyth, T. A. (2019). CFD flow dynamics over model scarps and slopes. *Physical Geography*, 00(00):1–24.

Heus, T., van Heerwaarden, C. C., Jonker, H. J. J., Pier Siebesma, A., Axelsen, S., van den Dries, K., Geoffroy, O., Moene, A. F., Pino, D., de Roode, S. R., and Vilà-Guerau de Arellano, J. (2010). Formulation of and numerical studies with the Dutch Atmospheric Large-Eddy Simulation (DALES). *Geoscientific Model Development Discussions*, 3(1):99–180.

Hoonhout, B. and van Thiel de Vries, J. (2014). Invloed van strandbebouwing op zandverstuiving.

Huybrechts, P. (2013). Cryosphere. *Encyclopedia of Earth Sciences Series*, pages 1030–1032.

Judice, S. F., Coutinho, B. B. S., and Giraldi, G. A. (2007). A Cellular Automata Framework for Real Time Fluid Animation. *Work*, (January):2–9.

Lavell, A., Oppenheimer, M., Diop, C., Hess, J., Lempert, R., Li, J., Muir-Wood, R., and Myeong, S. (2012). Climate change: New dimensions in disaster risk, exposure, vulnerability, and resilience. *Managing the Risks of Extreme Events and Disasters to Advance Climate Change Adaptation: Special Report of the Intergovernmental Panel on Climate Change*, 9781107025:25–64.

Martinez, C., Castillo, O., and Montiel Ross, O. (2008). Comparison between ant colony and genetic algorithms for fuzzy system optimization. volume 154, pages 71–86.

Mikami, M., Yamada, Y., Ishizuka, M., Ishimaru, T., Gao, W., and Zeng, F. (2005). Measurement of saltation process over gobi and sand dunes in the taklimakan desert, china, with newly developed sand particle counter. *Journal of Geophysical Research: Atmospheres*, 110(D18).

Mouret, G. (2012). Etude de la sensibilite d'une solution numerique aux parametres incertains ou inconnus : applications aux ecoulements turbomachines.

Nickling, W. G. and Neuman, C. M. (2009). Aeolian sediment transport. In Parsons, A. J. and Abrahams, A. D., editors, *Geomorphology of Desert Environments*, chapter 17, pages 517–555.

Nordstrom, K., Bauer, B., Davidson-Arnott, R., Gares, P., Carter, R., Jackson, D., and Sherman, D. (1996). Offshore aeolian transport across a beach: Carrick finn strand, ireland. *Journal of Coastal Research*, 12:664–672.

Nüst, D., Granell, C., Hofer, B., Konkol, M., Ostermann, F. O., Sileryte, R., and Cerutti, V. (2018). Reproducible research and giscience: an evaluation using agile conference papers. *PeerJ*, 6.

Oxman, R. (2008). Performance-based design: Current practices and research issues. *International Journal of Architectural Computing vol. 6 - no. 1, pp. 1-17*, 6.

Parente, A., Gorlé, C., van Beeck, J., and Benocci, C. (2011). Improved k– model and wall function formulation for the rans simulation of abl flows. *Journal of Wind Engineering and Industrial Aerodynamics*, 99(4):267–278. The Fifth International Symposium on Computational Wind Engineering.

Piomelli, U. (2014). Large eddy simulations in 2030 and beyond. *Philosophical Transactions of the Royal Society A: Mathematical, Physical and Engineering Sciences*, 372(2022).

Santer, T. J., Williams, B. J., and Notz, W. I. (2018). *Design and analysis of computer experiments*.

Schaffer, J. D., Caruana, R. A., Eshelman, L. J., and Das, R. (1989). A study of control parameters affecting online performance of genetic algorithms for function optimization. *Proceedings of the third international conference on Genetic algorithms*, (January).

Schultz van Haegen, M.H., M. v. I. e. M. (2017). Kustpact. pages 1–20.

Smyth, T. A. (2016). A review of Computational Fluid Dynamics (CFD) airflow modelling over aeolian landforms. *Aeolian Research*, 22:153–164.

Talamelli, A., Riparbelli, L., and Westin, J. (2004). An active grid for the simulation of atmospheric boundary layers in a wind tunnel. *Wind and Structures*, 7.

Thet, M. S. and San, Y. K. (2017). Comparison of Turbulence Models for Computational Fluid Dynamics Simulation of Wind Flow on Cluster of Buildings in Mandalay. *International Journal of Scientific and Research Publications*, 7(8):337–350.

Valen-Sendstad, K., Mortensen, M., Langtangen, H. P., Reif, B. A. P., and Mardal, K.-A. (2013). Implementing a k-ϵ Turbulence Model in the FEniCS Finite Element Programming Environment. (October):13.

van Bergen, J., Mulder, J., Nijhuis, S., Poppema, D., Wijnberg, K., and Kuschnerus, M. (2021). Urban dunes - towards bwn design principles for dune formation along urbanized shores. *Research in Urbanism Series*, 7 (2021):101–128.

van Onselen, E. P. (2018). Analysing measures to improve beach - dune interaction in the presence of man - made structures using computational fluid dynamics (CFD). (June).

Wang, B. (2015). Les impacts de la morphologie urbaine sur le vent : performance d ' énergie éolienne à l ' échelle de quartier To cite this version : HAL Id : tel-01245149.

Colophon

This document was typeset using LaTeX, using the KOMA-Script class `scrbook`. The main font is Palatino.